PETROGRAPHY AND GEOCHEMISTRY OF CONTINENTAL CARBONATES IN SOUTH TEXAS: IMPLICATIONS FOR OLIGOCENE-MIOCENE PALEOCLIMATE AND PALEOENVIRONMENT NEAR SEA LEVEL

by

CONAN GODFREY

Presented to the Faculty of the Graduate School of

The University of Texas at Arlington in Partial Fulfillment

of the Requirements

for the Degree of

MASTER OF SCIENCE IN GEOLOGY

PETROLEUM GEOSCIENCE OPTION

THE UNIVERSITY OF TEXAS AT ARLINGTON

May 2017

Acknowledgements

I thank Dr. Majie Fan for the guidance and support, Dr. Elizabeth Griffith and Dr. Merlynd Nestell for the advice and revisions, Lu Zhu, Min Gao, and Ohood Bader AlSalem for timely suggestions and recommendations in the lab, and Ellie Brown for help in the fieldwork.

April 24, 2017

Abstract

PETROGRAPHY AND GEOCHEMISTRY OF CONTINENTAL CARBONATES IN SOUTH TEXAS: IMPLICATIONS FOR OLIGOCENE-MIOCENE PALEOCLIMATE AND PALEOENVIRONMENT NEAR SEA LEVEL

Conan Godfrey, MS

The University of Texas at Arlington, 2017

Supervising Professor: Majie Fan

The Oligocene-Miocene Catahoula, Oakville, and Goliad formations in south Texas contain abundant continental carbonates which are useful in reconstructing paleoclimate and paleoenvironment in a near sea level region. Field observations and thin section characterizations identify three types of pedogenic carbonates, including rhizoliths, carbonate nodules, and platy horizons, and two types of groundwater carbonates, including cemented beds and carbonate concretions. The pedogenic carbonates display sharp upper contacts and diffuse lower contacts, and contain soil structural elements and biogenic elements related to root action. Under microscope, the pedogenic carbonates are micritic with clotted micrite, micrite laminations, and alveolar-septal structures and display dull cathodoluminescence. The groundwater carbonates display sharp lower contacts and preferential cementation within permeable units, and lack pedogenic profiles that destroy original beddings. Under microscope, the groundwater carbonates contain equant, blocky and sometime drusy and poikilotopic spars, and the spars often display dull to bright orange concentrically-zoned cathodoluminescence. Based on the preservation of microfabrics and the variabilities of carbon and oxygen stable isotopic compostion, we suggest that all the studied carbonates experienced minimal diagenesis, and their isotopic compositions

reflect paleoclimate and paleoenviornment in south Texas during the Oligocene and Miocene. The $\delta^{18}O$ values of the continental carbonates decreased ~3 ‰ after the earliest Oligocene, which is interpretted to reflect at least a 6° C drop in mean annual temperature in south Texas. The $\delta^{13}C$ values of the pedogenic carbonates increased ~4.4 ‰ from the late Oligocene to the middle Miocene, suggesting an expansion of C_4 plants in south Texas as early as the early Miocene. This early Miocene expansion of C_4 plants is ~16 myr older than what has been documented in Asia, possibly as a result of local climate change rather than global climate change.

Table of Contents

Acknowledgements iii

Abstract iv

List of Illustrations viii

Introduction 1

Stratigraphy and Ages 4

Analytical Methods and Results 9

Petrographic and XRD analysis 10

Stable isotope analysis 11

Description and Interpretation of Authigenic Carbonates 12

Pedogenic carbonates 12

Rhizoliths 12

Pedogenic carbonate nodules 17

Platy horizons 21

Groundwater carbonates 24

Cemented beds 24

Groundwater carbonate concretions 28

Discussion 31

1. Isotopic differences among different types of carbonates 32

2. Changes in paleoclimate during the Oligocene and Miocene 36

3. Changes in paleoenvironment during the Oligocene and Miocene 39

Conclusions 41

Appendix A Stable Isotope Results 43

Appendix B Measured Sections 48

References 57

Biographical Information..71

List of Illustrations

Figure 1: Sample locations 5

Figure 2: Composite stratigraphic column 6

Figure 3: XRD results 11

Figure 4: Rhizoliths in outcrop 13

Figure 5: Photomicrographs of rhizoliths 15

Figure 6: Nodular and platy horizons in outcrop 18

Figure 7: Photomicrographs of pedogenic carbonate nodules 19

Figure 8: Photomicrographs of platy horizons 22

Figure 9: Groundwater carbonates in outcrop 25

Figure 10: Photomicrographs of cemented beds 26

Figure 11: Photomicrographs of groundwater concretion 30

Figure 12: Carbon and oxygen isotope crossplots 33

Figure 13: Isotopic compostion with depth within soil profiles 34

Figure 14: Change in carbonate $\delta^{18}O$ and δ13C values through time 37

Introduction

Continental climatic and environmental responses to global climate changes are increasingly important to the understanding of landscape evolution (e.g., Ramstein et al., 1997; An et al., 2001; Dupont-Nivet et al., 2007), faunal evolution (e.g., Bowen and Bloch, 1997; Sun et al., 2014), and paleoenvironmental changes (e.g., Quade and Roe, 1999; Bowen et al., 2008; Fox et al., 2012a; 2012b; Singh et al., 2012). Well-studied marine geologic records have shown that Earth's climate was cold during most of the Oligocene, became warmer during the latest Oligocene and early Miocene, and then experienced gradual cooling after the middle Miocene (Zachos et al., 2001). Current understanding of middle and late Cenozoic climatic and environmental changes in the continental realm show heterogonous responses to global climatic events, depending on latitude and altitude of the study sites and proxies used for such reconstructions (e.g., Hooker et al., 2004; Eronen et al., 2015; Sheldon et al., 2016). In North America, continental records of the Oligocene-Miocene periods are mainly from the mid-latitude of western U.S.A., and the reconstructed paleoclimates are not well correlated with global events. For example, paleosol geochemistry studies show that mean annual precipitation (MAP) and temperature (MAT) remained stable in the northern Rocky Mountains across the global cooling at the Eocene-Oligocene boundary, and during the late Neogene global

cooling (Sheldon and Retallack, 2004; Retallack et al., 2007). A recent study using volcanic glass hydrogen isotope (δD) values suggests gradual drying occurred during the Oligocene-Miocene in the central Rocky Mountains and its adjacent Great Plains (Fan et al., 2014a). Additionally, reconstructed mean warm-season temperature dropped ~8 to 10 °C after the late Miocene on the Colorado Plateau and in the central Rocky Mountains (Huntington et al., 2010; Fan et al., 2014b; Mix and Chamberlain, 2014) showing remarkable response to late Neogene global cooling. These observations suggest that topography of the Rocky Mountains may have masked continental climate responses to various degrees in the western U.S. (e.g., Chase et al., 1998; Retallack et al., 2007), and call for studies of continental climate in low elevation coastal regions.

Carbonate stable isotope compositions are important proxies of continental climate and environments (e.g., Cerling and Quade, 1993; Dworkin et al., 2005; Sanyal et al., 2005). Interpretation of stable isotope records, however, requires comprehensive understanding of depositional and diagenetic processes of the carbonates (e.g., Bowen and Bloch, 1997; Mack et al., 2000; Hall et al., 2004; Quast et al., 2006; Bowen et al., 2008). For example, carbonates formed in different depositional settings may record seasonal or annual climatic conditions (Breecker et al., 2009; Hough et al., 2014); diagenetic carbonate precipitation may overprint the isotopic information that is representative to the climate and environmental conditions during the deposition of sediment. Therefore, careful

carbonate characterization and assessment of diagenesis must be conducted in order to use continental carbonates for paleoclimate and paleoenvironmental reconstructions.

The objective of this study is twofold. First, I conduct outcrop, petrographic, and stable isotopic characterization of continental carbonates in the Oligocene-Miocene fluvial successions in south Texas in order to understand depositional and any potential diagenetic processes of these carbonates. Second, I use the stable isotopic compositions of unaltered carbonates to reconstruct paleoclimate and paleoenvironments in a near sea level region. Aggradation of rivers in the coastal plain in south Texas formed the Catahoula, Oakville, and Goliad formations, which contain abundant continental carbonates, providing an opportunity to study near sea-level, low-latitude continental climatic responses throughout the middle and late Cenozoic. In this region, lack of influence of continentality and altitude on meteoric water isotopic compositions potentially makes interpretation of paleoclimate from carbonate isotopic compositions straightforward. Additionally, recent studies of stable isotopic compositions of Quaternary pedogenic carbonates (Zhou and Chafetz, 2010) and modern water (e.g., Kendall and Coplen, 2001; Pape et al., 2010) provide a basis for interpreting the carbonate isotopic data.

Stratigraphy and Ages

The Texas Gulf Coast is part of a passive, divergent continental margin, which has been shaped by the interaction of eight fluvial dispersal axes associated with separate, structurally defined entry points and sediment sources during the middle and late Cenozoic (Galloway et al., 2000). The study area in south Texas includes Duval, Live Oak, Bee, Karnes, and Goliad counties located within the modern-day Rio Grande embayment that extends south from the San Marcos arch (Fig. 1) (Galloway, 1977). The outcrops of the Oligocene-Miocene strata in the study area are distributed in concentric bands striking northeast to southwest (Figure 1).

The strata dip slightly to southeast, and thus become progressively younger toward the coast. The depositional environment in the region generally changed from strand plain-beach systems in the late Eocene, to the Gueydan fluvial axis in the Oligocene, the George West fluvial axis in the early to middle Miocene (Galloway, 1977), and the relict Nueces fluvial axis by the middle to late Miocene (Solis, 1981). This study focuses on the Oligocene-Miocene strata (Fig. 2), and below I briefly summarize the stratigraphy and age constraints.

The Catahoula Formation is at most 255 m thick in outcrop, and is composed of tuffaceous claystone, sandstone, and conglomerate with a few beds of vitric ash (McBride et al., 1968). Bailey (1926) divided the formation into three subunits based on variations in lithologic composition, including the Fant tuff,

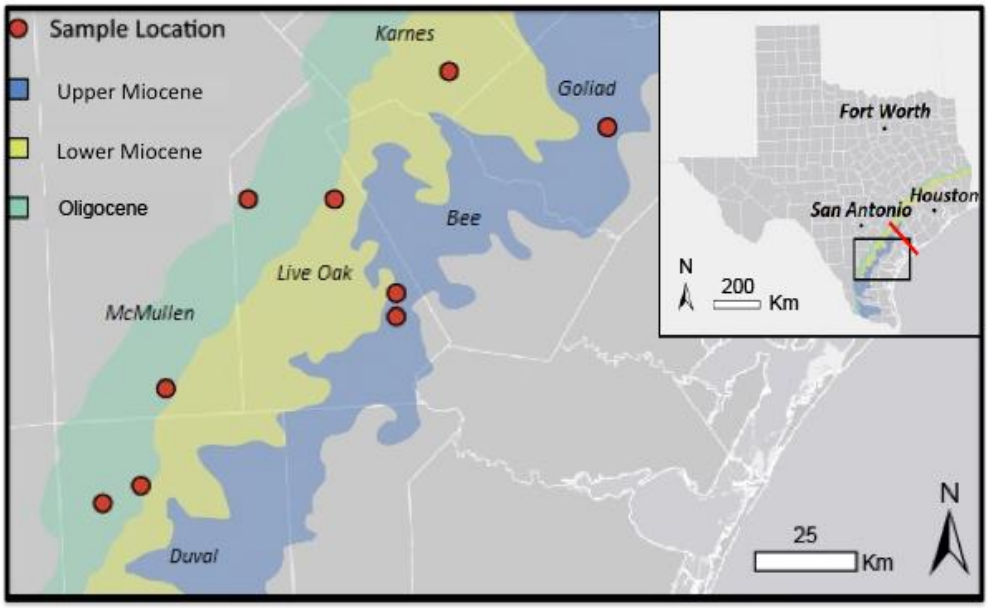

Figure 1: Sample locations and distribution of the Oligocene-Miocene sedimentary rocks in south Texas coastal plain Southwest of the San Marcos Arch (red line), within the Rio Grande Embayment.

Soledad sandstone, and Chusa tuffaceous clay subunits from the base to the top. The white to very light gray Fant tuff subunit contains a basal faintly-bedded sandstone that contains up to 60% glass shards, and the other grains are quartz, plagioclase, volcanic rock fragment, and detrital carbonates (McBride et al., 1968). The upper part of the subunit contains pisolitic textures and irregular lumpy masses that are typically of pedogenic origin (McBride et al., 1968). The Soledad subunit is up to 25 m thick, and not laterally continuous. The subunit contains sandy conglomerate, pebbly sandstone, and sandstone, and the clasts in

conglomerate and the framework grains in sandstone are predominantly

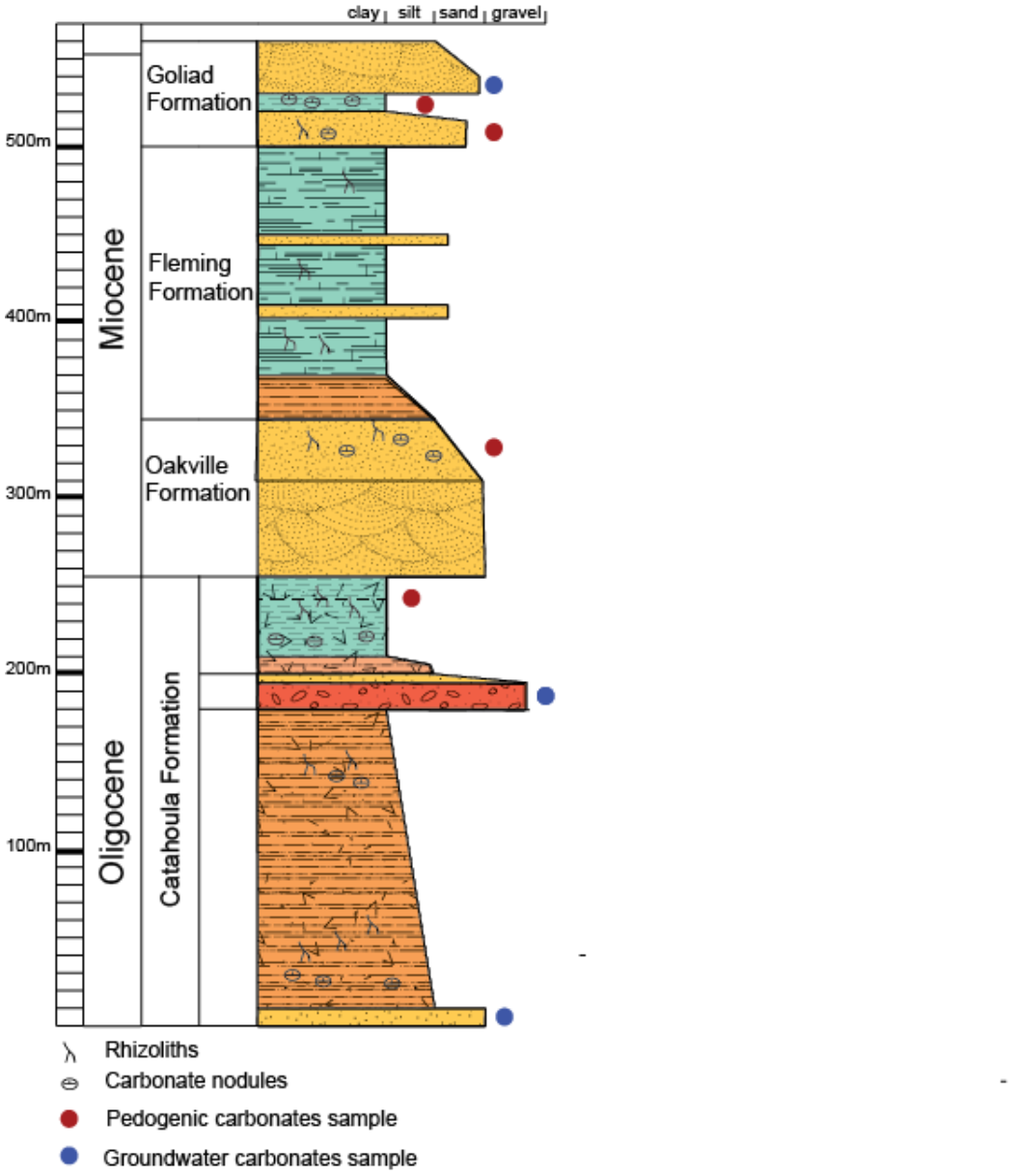

Figure 2**:** Composite stratigraphic column showing sampled intervals

conglomerate and the framework grains in sandstone are predominantly composed of volcanic rock fragments and recycled silicified claystone with a minor amount of chert (McBride et al., 1968). The Chusa tuffaceous clay subunit contains predominantly light gray to pink tuffaceous claystone with abundant recycled clay granules, and floating sand grains. The subunit contains abundant caliche, pisolites, concretions, and is lacking bedding (McBride et al., 1968). The sandstone contains less carbonate detritus than the sandstone in the Fant tuff subunit (McBride et al., 1968). The Catahoula Formation was interpreted to be deposited in a fluvial depositional system with associated floodplain, channel-fill, crevasse-splay, and interchannel lakes (Galloway, 1977). The Catahoula Formation was correlated down dip to the Frio Formation in subsurface, which contains fossil foraminiferal assemblages including *Textularia warreni*, of Oligocene age (Deussen and Owen, 1939). Sanidine $^{40}Ar/^{39}Ar$ dating of an ash bed in the basal Catahoula Formation yielded an age of 30.654 ± 0.055 Ma (Heintz et al., 2015), confirming the depositional age of middle Oligocene. The top of the Catahoula Formation was correlated down dip to the sandstone above the Frio Formation in subsurface, which contains fossil foraminiferal assemblages including *Heterostegina texana* and *Marginulina texana* (Galloway, 1982), both are of the Chattian stage of the late Oligocene (Ewing and Reed, 1984).

The Oakville Formation is approximately 90 m thick in outcrop. The formation contains light buff to light gray, massive or cross-bedded, medium-

grained sandstone with more than 50% of the grains are detrital carbonates and recycled Cretaceous marine fossils (Galloway, 1982). The Oakville Formation was interpreted to be deposited by a braided river system containing multiple anastomosing sand bodies (Galloway, 1982). The sand-rich Oakville Formation grades both laterally and up-section into the Fleming Formation, which contains predominantly calcareous claystone that were deposited in floodplains. The Fleming Formation is about 155 m thick and occasionally contains cross-bedded sandstone lenses and carbonate concretions (Sellards et al., 1932). An early to middle Miocene age was determined based on the presence of marine bivalve, scaphopod, and gastropod assemblages, including *Leda sp., Pecten sp., Cardium sp., Tellina sp., Corbula sp., Dentalium sp., Cadulus sp., Adeorbis sp., Architectonic sp., Natica sp., Polynices sp., Turritella sp., Alectrion sp., Oliva sp., Cancellaria sp., and Drillia sp*. from the down dip equivalent of the Fleming Formation in the subsurface east of Brownsville in southern Cameron County (Sellards et al., 1932). Vertebrate fossils including *Protohippus medius, Protohippus perditus, Protohippus placidus, and Aphelops meridianus*, in outcrops of the Oakville Formation along the Nueces River in Live Oak County also confirm the middle Miocene depositional age (Sellards et al., 1932).

The Goliad Formation is around 60 m thick and composed of interbedded sandstone and claystone (Sellards et al., 1932; Eargle, 1971). The sandstone units are gray to white, calcareous, massive or cross-bedded, and occasionally contain

basal conglomerate (Sellards et al., 1932; Eargle, 1971). The sandstone units in this formation contain more chert and feldspar grains than the underlying Fleming Formation. The claystone units are gray to pink, massive, and occasionally contain carbonate nodules (Sellards et al., 1932; Eargle, 1971). The Goliad Formation was interpreted to be deposited in anastomosing braided rivers and associated floodplains that grade down dip into a meandering river (Solis, 1981). The base of the formation was determined to be middle Miocene in age based on down dip correlation to the Amphistegina B shale in subsurface (Galloway et al., 1986). The top of the formation was determined to be middle Miocene to earliest Pliocene, based upon vertebrate fossil assemblages containing *Ceratogaulus cf. anecdotus, Pseudhipparion skinneri, Cormohipparion cf. ingenuum, and Calippus cf. cerasinus* that corresponds to Clarendonian North American Land Mammal stage (Basken and Hulbert, 2012).

Analytical Methods and Results

Samples were collected from 8 locations in the Catahoula, Oakville, and Goliad formations distributed in Duval, Live Oak, Bee, Karnes, and Goliad Counties. Twelve representative samples of each type of carbonate identified in this study were slabbed and 30-μm-thick standard-sized thin sections were produced using kerosene as lubricant with a 0.05 μm polish. The twelve samples were pulverized using a ceramic mortar and pestle for carbonate species

determination using X-ray diffraction (XRD) analysis. Oxygen and carbon stable isotopic compositions were analyzed from 123 samples taken from the slabs, and 33 bulk samples taken from hand specimens.

Petrographic and XRD analysis

Cathodoluminescence (CL) of the thin sections was performed at The University of Texas at Arlington Carbonate Characterization Laboratory using a Reliotron Cold Cathode Ray device, which was operated at 7-9 kV and 0.3-0.5 mA. The device is connected to a Leica petrographic microscope and camera. Observations of luminescence were interpreted according to Machel and Burton (1991). Thin sections were also examined using the Leica petrographic microscope for characterization of carbonate microfabrics. The results of petrographic observations were used to classify carbonates and interpret the origin and formation mechanism.

XRD analysis was performed at the Shimadzu Center for Environmental, Forensics, and Material Science in The University of Texas at Arlington using a Shimadzu 7000. The XRD patterns were obtained while the instrument was operated at 45 kV and 45 mA. Samples were scanned from 25° to 55° 2θ at 0.02° increments to focus on the interpretation of carbonate mineralogy. All 12 samples analyzed were determined to be composed of calcite (Figure 3).

Stable isotope analysis

Samples used for isotope analysis were examined with a microscope to assist in selective sampling in order to avoid areas that experienced potential diagenesis. Targeted areas of analysis were drilled from hand specimens using a hand-held Dremel or slabs using a New Wave Micromill based on petrographic

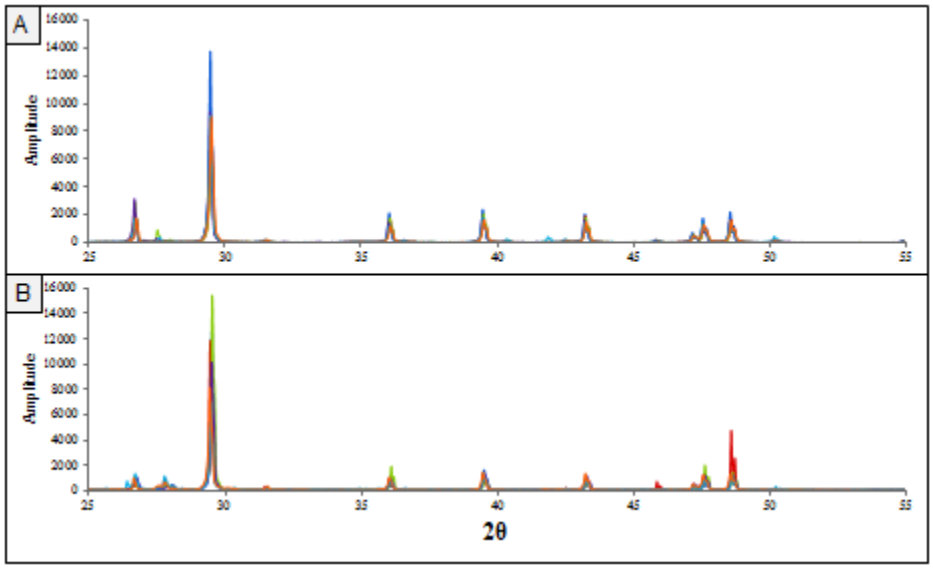

Figure 3: XRD results from (A) 6 Miocene samples and (B) 6 Oligocene samples.

and CL observations of different carbonate texture. Carbonate $\delta^{18}O$ and $\delta^{13}C$ values were measured using a Gasbench connected to a Delta-V Advantage Isotope Ratio Mass Spectrometer at The University of Texas at Arlington, and the isotope values were calibrated using NBS 18 and NBS 19, and reported in δ notation relative to Vienna PeeDee Belemnite (VPDB). The precision of both isotopic measurements are better than 0.15‰ (1σ). The $\delta^{18}O$ values range from -2.9 ‰ to -5.8 ‰, and the $\delta^{18}O$ values from the same stratigraphic intervals range

up to 2.6 ‰. The $\delta^{13}C$ values range from -9.7 ‰ to -3.0 ‰, and the $\delta^{13}C$ values from the same stratigraphic intervals range up to 5.1 ‰ (Appendix A).

Description and Interpretation of Authigenic Carbonates

Field and microscopic observations place the studied Oligocene and Miocene continental carbonates in south Texas into two categories, pedogenic carbonates and groundwater carbonates. Pedogenic carbonates are further divided into rhizoliths, nodules, and platy horizons, and groundwater carbonates are further divided into carbonate-cemented beds and carbonate concretions based on physical characteristics in outcrops and microfabrics observed in thin sections. Below I summarize the observations and interpret the formation mechanism of each type of carbonate.

Pedogenic carbonates

Rhizoliths

In outcrops, rhizoliths include root mold, root tubule, rhizocretion, and root cast morphologies with diameters up to 1.5 cm (Figure 4). Root tubules and casts generally display downward branching and tapering. Rhizoliths of horizontal, oblique, and vertical orientations were commonly observed in pedogenic carbonate nodular and platy horizons, but sometime occur in massive sandstone and mudstone or sandstone with some degree of preservation of

original sedimentary structures (Figure 4A-C). Rhizoliths are also present in beds overlying carbonate concretions in the Fant tuff subunit of the Catahoula Formation (Figure 4D). In this case, horizontal to sub-horizontal groups of root casts, called root mats (Wright et al., 1995; Alonso-Zarza, 1999), overlying

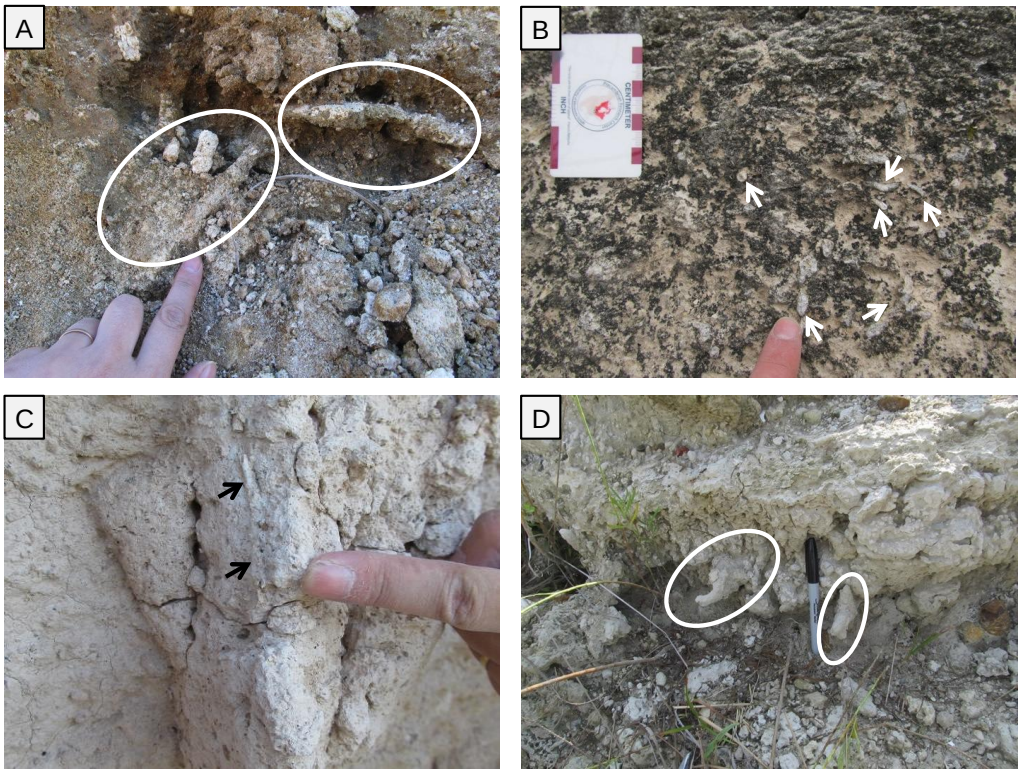

Figure 4: Rhizoliths in outcrops. (A) Oblique and horizontal root casts (in white circles) in the Oakville Formation. (B) Rhizocretions of ~0.5 cm in diameter (white arrows) in the lower portion of the Goliad Formation. (C) A vertical root tubule of ~0.5 cm in diameter (black arrows) within a tubular, vertically elongated pedogenic nodule in the Chusa subunit of the Catahoula Formation. (D) Horizontal root casts (in white circles) in the Fant tuff subunit of the Catahoula Formation.

groundwater carbonate concretions. Under microscope, this type of carbonate commonly contains alveoloar-septal structures with ramifying micrite walls, and

root molds are represented by voids (Figure 5). Rhizocretions are composed of micritic laminations and infilled with detrital aggregate grains. The alveolar-septal structures present within rhizocretions and root tubules contain needle fiber calcite in their centers (Figure 5D). Rhizoliths display very dull, or faint luminescence within the micritic laminations and bright orange luminescence only occurs in detrital carbonate grains (Figure 5B). The $\delta^{18}O$ and $\delta^{13}C$ values taken from a number of rhizoliths in the same stratigraphic level are variable, up to 0.7 ‰ and 1.8 ‰, respectively. Micritic laminations in a rhizocretion sample taken from the Goliad Formation were micromilled at various distances from the rhizocretion void in order to show the variations of stable isotope values within the same rhizocretion. The results show that the $\delta^{18}O$ and $\delta^{13}C$ values range up to 1.1 ‰ and 1.8 ‰, respectively (Figure 5E and 5G).

Rhizoliths observed in south Texas are similar to what have been summarized in Klappa (1980), indicating deposition of soil carbonates during the activity and decay of plant roots (Klappa, 1980; Retallack, 2001). Alveoloar-septal structures are carbonate-filled tubes representing the physico-chemical processes of root activities in vadose settings (James, 1972; Rabenhorst and Wilding, 1986; Alonso-Zarza and Wright, 2010). Needle fiber calcites are interpreted to be of fungal origin during root decay (e.g., Phillips and Self, 1987, Alonso-Zarza and Wright, 2010). Decomposition of root biofilm may lead to disaggregation of the needle crystals (Alonso-Zarza, 1999). The micritic walls of

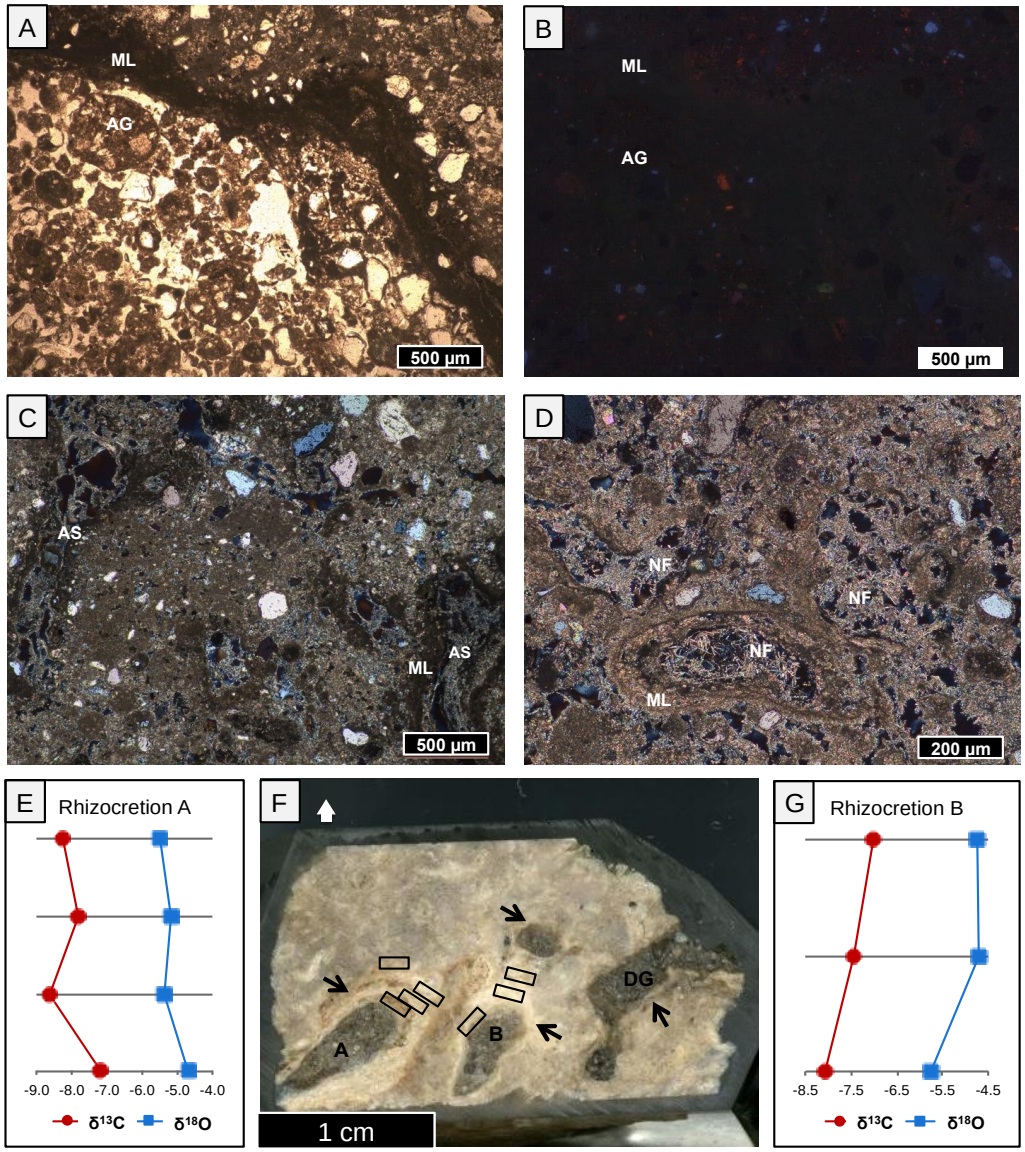

Figure 5: Photomicrographs of rhizoliths from the lower portion of the Goliad Formation. (A) Rhizocretion composed of micritic lamina (ML) and detrital grains and aggregate grains (AG) in plain light. (B)Same picture as A, but with cathodoluminescence. (C) Rhizocretions coated with micritic lamina (ML) and alveolar-septal structure (AS) with ramifying micrite walls in cross-polarized light. Black voids are root molds. (D) Close look of the oblique section through an alveolar-septal structure displaying needle fiber calcite (NF) coated with micritic laminations (ML) in plain light. (E) $\delta^{18}O$ and $\delta^{13}C$ values of laminated micrite sampled at various distances (black boxes) from the center of rhizocretion A showing in F. (F) Four bifurcating rhizocretions of 5-10 mm in diameter are composed of laminated micrite (black arrows) and infilled by detrital grains (DG). Arrow denotes upward direction. (G) $\delta^{18}O$ and $\delta^{13}C$ values of laminated micrite sampled at various distances (black boxes) from the center of rhizocretion B showing in F. Isotope values were reported in δ notation relative to VPDB.

the alveoloar-septal structures and the micritic laminae were produced from extracellular calcification caused by bacteria and fungi in mucigel and rhizosphere (Wright et al., 1995; Retallack, 2001). Therefore, this type of carbonate was formed in association with root activities in soil where plants disrupted the original sedimentary structures and the growth of soil carbonates displaced and replaced the host sediments and roots. However, the root mats in the Fant tuff subunit may be influenced greatly by groundwater because they probably formed in near-surface sandy sediment that was periodically waterlogged (Mack et al., 2000). The dull or faint luminescence is caused by low level of Mn^{2+}, which activates orange luminescence, in oxygenated environments within the vadose zone (Machel and Burton, 1991). The variations in $\delta^{18}O$ values should reflect changes in soil water $\delta^{18}O$ values and carbonate precipitation temperature (Kim and O'Neil, 1997), and various degree of evaporation of soil water $\delta^{18}O$ as a function of soil depth and lithology (e.g., Cerling and Quade, 1993; Breecker et al., 2009). The variations in $\delta^{13}C$ values should reflect changes in carbonate formation temperature (Romaneck et al., 1992), dominant plant types (C_3 vs. C_4), aridity, and addition of atmosphere CO_2 as a function of soil depth and lithology (e.g., Cerling and Quade, 1993; Breecker et al., 2009). The ranges of variation within the same stratigraphic level or same rhizocretion suggest change in at least one of the aforementioned factors in seasonal or decadal scales.

Pedogenic carbonate nodules

In outcrops, pedogenic carbonate nodules, with diameters ranging from 0.5-8 cm, are distributed within massive fine-grained sandstone and mudstone (Figure 6). The nodules vary in degree of induration from random, diffuse distribution with low carbonate to host material ratio, corresponding to the stage II soil carbonates in Giles et al. (1966) (Figure 6A), to dense distribution with high micrite to host material ratio, corresponding to the stage IV soil carbonates (Gile et al., 1966) (Figure 6B-D). The nodule-bearing horizons display gradational lower contacts and sharp upper boundaries (Figure 6B-C). In some cases, such as in the middle and upper portion of the Goliad Formation, stage II-IV nodular horizons are truncated by channel sandstone bodies. In other cases, such as in the Chusa subunit and lower portion of the Goliad Formation, the nodular horizons are overlain by another nodular profile or capped by platy horizons (Figure 6D-E). Under microscope, this type of carbonate contains abundant etched detrital grains and clotted micrite surrounded by microspars (Figure 7). Rootlet casts are common in well-developed nodules of stage III or greater (Figure 7C). Detrital grains are commonly coated by micrite or microspars (Figure 7). The mud matrices often have cracks that have been partially filled with fine spars (Figure 7E-F). The nodules display variable degree of luminescence, with bright orange or red luminescence spatially intermixed with dull

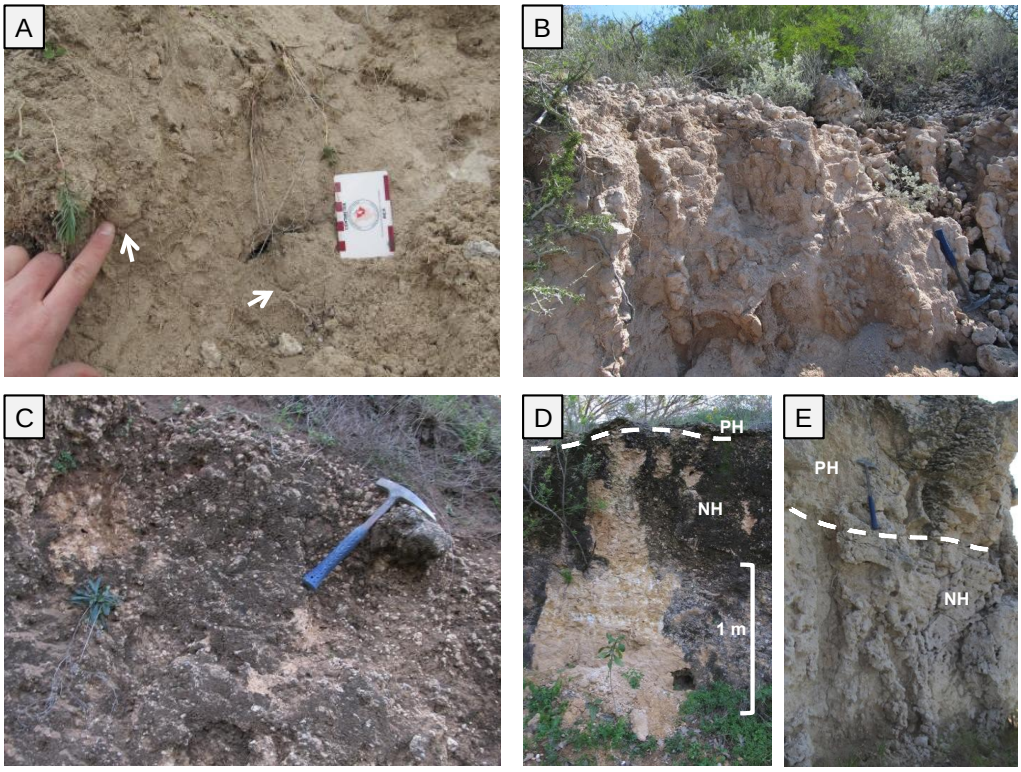

Figure 6: Pedogenic carbonate nodules in outcrops. (A) Diffuse nodules (pointed by white arrows) corresponding to stage II calcic soil profile development (Giles et al., 1966) in the Goliad Formation. (B) Well-developed nodules of 2-8 cm in diameter, corresponding to stage III calcic soil profile development in the Chusa subunit of the Cathoula Formation. This outcrop was truncated by a conglomerate lense, which is weathered to gravels. (C) Well-indurated nodules of 0.5-3 cm in diameter, corresponding to stage III calcic soil profile development in the Oakville Formation. (D) A nodular horizon (NH) caped by a thin platy horizon (PH) in the Oakville Formation corresponding to stage IV calcic soil profile development. (E) A nodular horizon (NH) caped by a thick platy horizon (PH) in the Chusa subunit of the Catahoula Formation, corresponding to stage V calcic soil profile development. Hammer is 42 cm in length.

luminescence in most of the area (Figure 7B and 7D). Detrital carbonate grains and microspars often display bright orange luminescence. The grain coating and fine-spars filling cracks typically have bright luminescence. The variation in

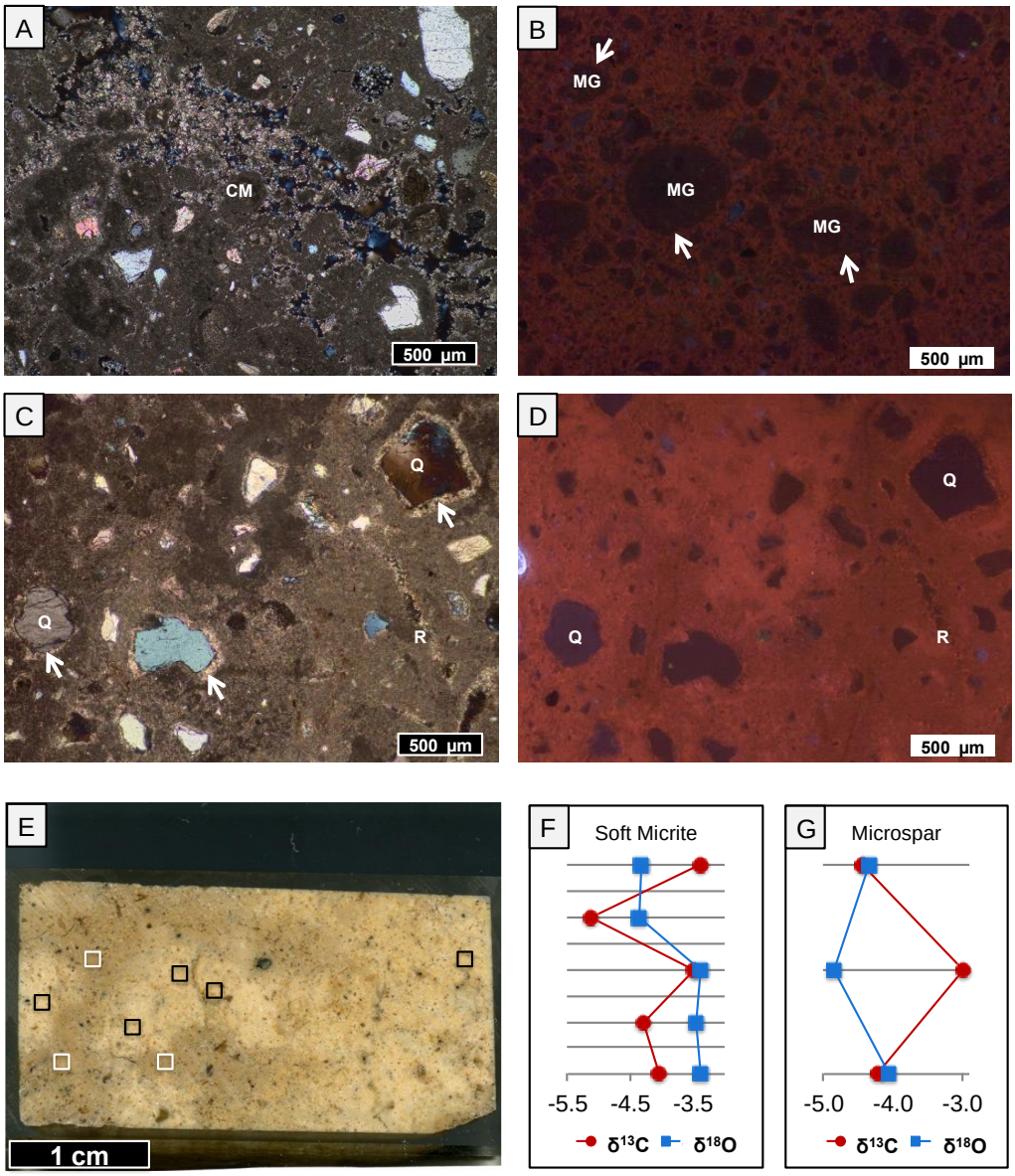

Figure 7: Photomicrographs of pedogenic carbonate nodules. (A) Clotted micrite texture (CM),and microspar- to spar-filled voids in the Oakville Formation in cross-polarized light. (B) Micrite granules (MG) rimmed by microspars from the Chusa subunit of the Catahoula Formation with cathodoluminescence. (C) Circumgranular cracks (white arrows) around detrital quartz (Q) filled with microspars and root cast (R) in the Goliad Formation in plain light. (D) Same picture as C, but with cathodoluminescence. (E) Slab bisecting nodules from the Oakville Formation. Samples collected from soft micrite (black boxes) and microspar-rich (white boxes) zones. (F) $\delta^{18}O$ and $\delta^{13}C$ values of soft micrite samples from E. G) $\delta^{18}O$ and $\delta^{13}C$ values of microspar-rich samples from E. Isotope values were reported in δ notation relative to VPDB.

degree of luminescence seems to be related to clay and organic matter contents (Figure 7C-D). The $\delta^{18}O$ and $\delta^{13}C$ values of subsamples micromilled from areas with variable luminescence range up to 1.5 ‰ and 2.2 ‰, respectively (Figure 7E-G).

The pedogenic carbonate nodules observed in south Texas are similar to what have been described in Giles et al. (1966), Machete (1985), and Bown and Krauss (1986), indicating formation in association with pedogenesis in soil B horizons (Retallack, 2001). The clotted micrite textures form by a combination of precipitation of micrite, and microfracturing of soil related to shrinkage and expansion (e.g., Bain and Foos, 2012). The circumgranular cracks around detrital grains that have been filled with microspar or micrite and cracks partially filled with fine spars are attributed to shrink-swell cycles related to frequent wetting and drying (Alonso-Zarza and Wright, 2010). The bright luminescence of carbonates coating detrital grains and filling cracks suggest they were formed in the phreatic zone when the water table was high and when water has high level of Mn^{2+} under reduced environment (Beckner and Mozley, 1998). Intermixed bright and dull luminescence suggests frequent variation of water tables during pedogenesis, or frequent changes in Ca^{2+} activity, and soil water chemistry because pH, rare earth element concentration in soil water, and calcite growth rate are other factors influencing carbonate luminescence (Machel and Burton, 1991). The variations in

stable isotopic compositions within the nodules were related to variations in soil water isotopic compositions, carbonate growth temperature, and addition of groundwater into soil water.

Platy horizons

In outcrops, platy horizons of 2 cm to 1 m thick occur only in fine-grained sandstone and cap nodular horizons (Figure 6D-E). Platy horizons are basically limestone beds with appearances of lamination or horizontal bedding and often contain horizontal or sub-horizontal rhizoliths. They have sharp upper contacts, but change to nodular horizons downward (Figure 6D-E). Under microscope, carbonates in platy horizons are characterized by horizontal to sub-horizontal microfabrics (Figure 8). The microfabrics are composed of alternating detrital grain-rich laminae and dense, wavy, and discontinuous micritic laminae or horizontal alveolar-septal structure of 10-50 μm thick (Figure 8). The micritic laminae have extremely dull red luminescence, and the detrital carbonates within the grain-rich laminae have bright orange luminescence (Figure 8B, D, F). The micritic laminae in a platy horizon in the upper portion of the Oakville Formation were micromilled to study variations of stable isotopic compositions. The $\delta^{18}O$ and $\delta^{13}C$ values range up to 0.6 ‰ and 1.5 ‰, respectively (Figure 8G-H). A couplet of platy horizon and underlying nodular horizon in the Chusa subunit of the Catahoula Formation was sampled every 25 cm and a couplet in the upper portion of the Oakville Formation was sampled every 50 cm to examine variations

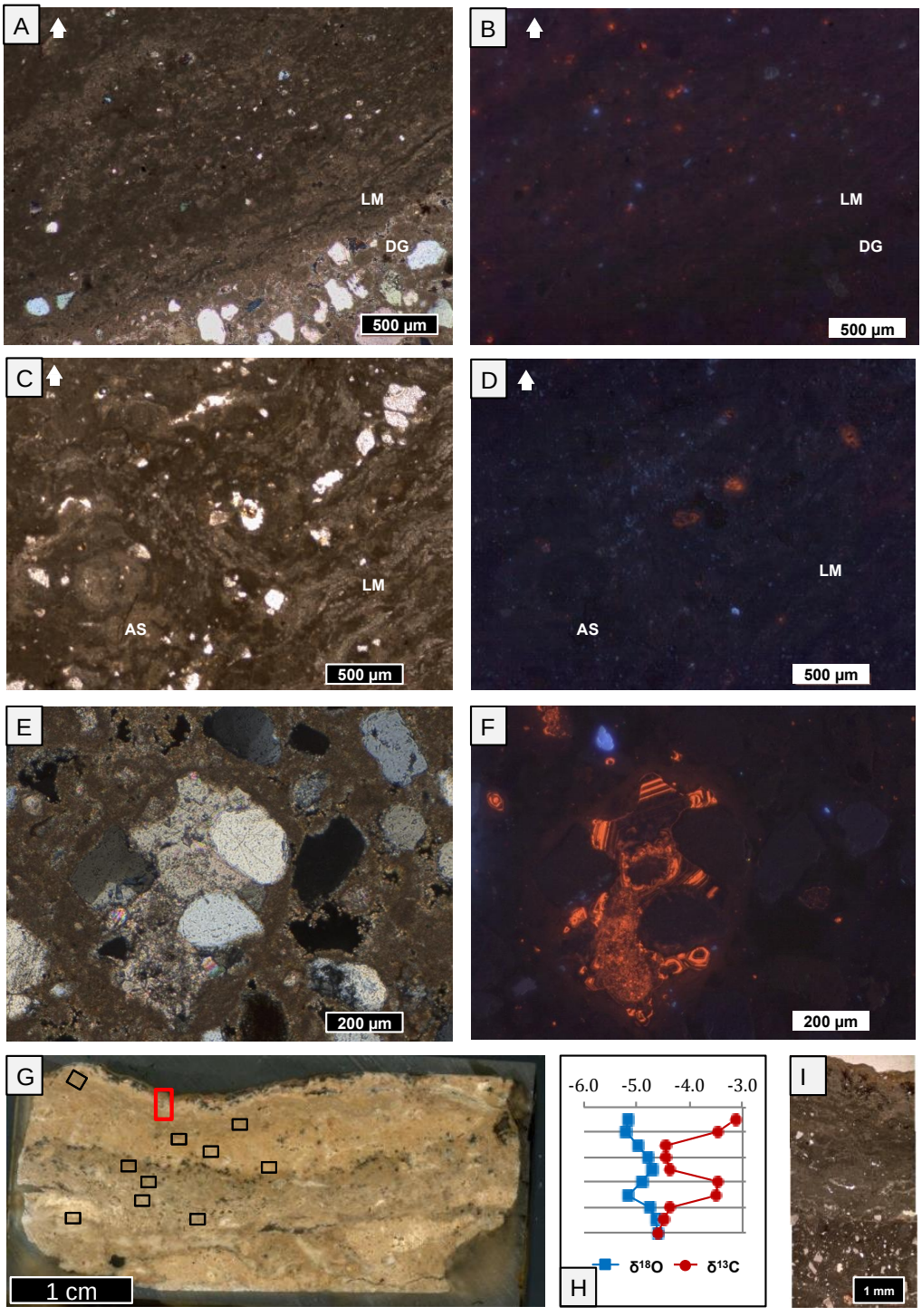
A
LM
DG
500 µm
B
LM
DG
500 µm
C
LM
AS
500 µm
D
LM
AS
500 µm
E
200 µm
F
200 µm
G
1 cm
-6.0
-5.0
-4.0
-3.0
δ18O
δ13C
H
I
1 mm

Figure 8: Photomicrographs of platy horizon carbonates. Arrow indicates upward direction. (A) Subhorizontal laminated micrite (LM) overlies detrital a grain-rich lamina (DG) in the Goliad Formation in cross-polarized light. (B) Same picture as A, but with cathodoluminescence. (C) Abundant laminated micrite (LM) and alveolar-septal structure (AS) in the Oakville Formation in cross-polarized light. (D) Same picture as C, but with cathodoluminescence. (E) A large detrital grain with carbonate cement is coated by micrite, and some voids (black area) with thin layers of microspar in their inner walls in cross-polarized light. Sample is from the Goliad Formation. (F) Same picture as D, but with cathodoluminescence. (G) Slab bisecting a platy horizon in the Oakville Formation. Note abundant laminations and micromill sampling locations (in black boxes). (H) Variations of $\delta^{18}O$ and $\delta^{13}C$ values along depth in the slab in G. (I) Alternation of micritic laminae and detrital grain-rich laminae from the slab in G indicated with a red box. Isotope values were reported in δ notation relative to VPDB.

of stable isotopic compositions. The $\delta^{18}O$ and $\delta^{13}C$ values of the Chusa couplet vary up to 1.3 ‰ and 1.3 ‰, respectively, and the values of the Oakville couplet range up to 1.5 ‰ and 1.9 ‰, respectively. An overall trend in isotopic compositions cannot be summarized from the two sites.

The platy horizon carbonates in south Texas are similar to the stages IV-V calcic soil carbonate described by Giles et al. (1966), Machette (1986), and Alonzo-Zarza and Wright (2010). Lack of original sedimentary structures coupled with spatial association with rhizoliths and nodular horizons indicate a pedogenic origin (Alonzo-Zarza and Wright, 2010). Platy horizons form because accumulation of soil carbonates within soil B horizons gradually decreases soil permeability, causing lateral development of root systems (Alonzo-Zarza and Wright, 2010). Continuous lateral carbonate accumulation by root systems not only produced the appearance of lamination or horizontal bedding in outcrop, but also laminated micrite and sub-horizontal alveolar-septal structure within detrital grain-rich intervals in thin section scale (Alonso-Zarza, 1999). Formation of platy

horizons requires a protracted period of landscape stability, thus they are present only in strata far away from major active fluvial channels (Alonso-Zarza and Wright, 2010). The dull red luminescence within the micrite and the lack of spars indicate formation of platy horizons in oxygenated environments in vadose zone with low Mn^{2+} concentrations (Machel and Burton, 1991). Small cyclic variations in the $\delta^{18}O$ and $\delta^{13}C$ values within the platy horizons and their underlying nodule horizons within the Chusa subunit of the Catahoula Formation and the Oakville Formation can be attributed to changes in soil water isotopic compositions, carbonate growth temperature, soil depth and lithology, aridity, and plant types.

Groundwater carbonates

Cemented beds

In outcrops, laterally extensive beds cemented by carbonate include massive or cross-bedded fine- to coarse-grained sandstone and poorly sorted, matrix-supported conglomerate lenses (Figure 9). The sandstone beds range from 1-2.5 m thick, forming weathering-resistant ledges. The conglomerate lenses are discontinuous and of 10-50 cm thick. These beds display sharp upper and lower boundaries, conforming to original bedding planes and are lacking of soil profile development (Figure 9A-C). Under microscope, the intragranular areas of the sandstone and conglomerate are mostly larger than 30% of the thin section surface area, and filled by carbonate cement, and the detrital grains are mostly in point and long contacts (Figure 10). The cements in the medium- to coarse-grained

sandstone and conglomerate are blocky, equant, with some interstitial spars of 30-500 μm in diameter. Single carbonate crystals infill the entire pore spaces in some cases. The cements in fine-grained sandstone contain microspars and fine spars (Figure 10). Detrital grains, including reworked mud and fine-grained tuff

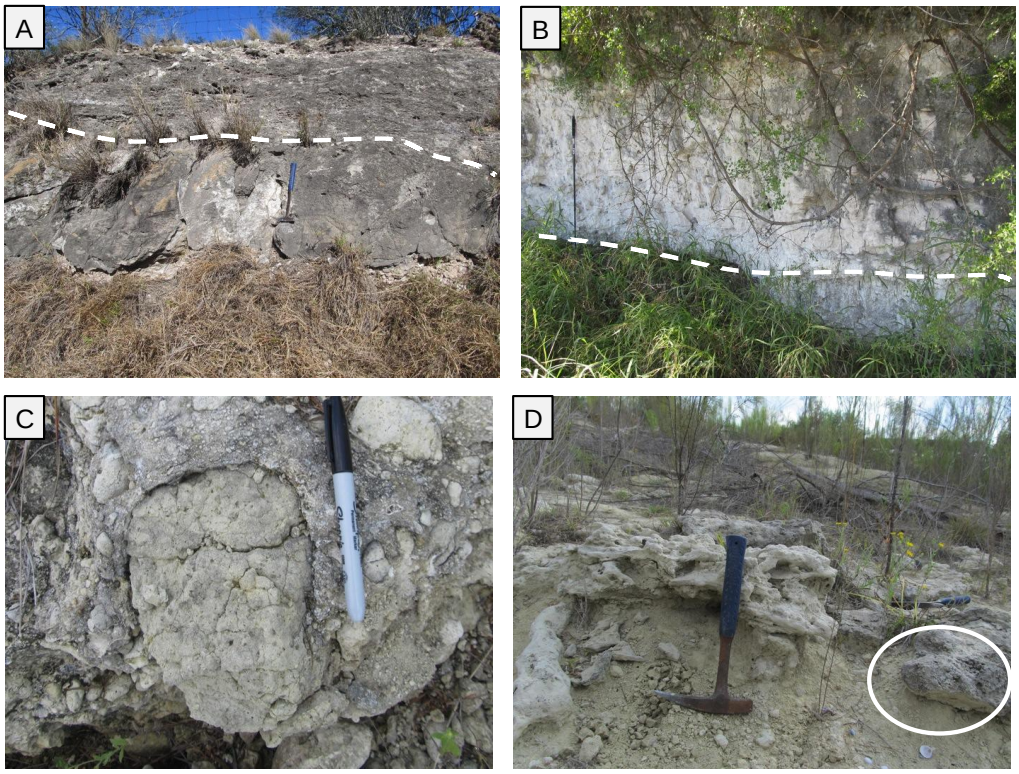

Figure 9: Photographs of ground water carbonates at outcrop scale. (A) Carbonate-cemented sandstone conforms to original bedding planes and has a sharp lower boundary. Site is in the Soledad subunit of the Catahoula Formation. Hammer is 42 cm in length. (B) Carbonate-cemented sandstone overlies a claystone bed in the upper portion of the Goliad Formation. Staff is 1.5 m in length. (C) A carbonate concretion in a poorly sorted conglomerate bed containing fine-grained sandstone intraclasts in the Fant tuff subunit of the Catahoula Formation. Marker is 12 cm in length. (D) Horizontally elongated groundwater concretion within the Fant tuff subunit of the Catahoula Formation.

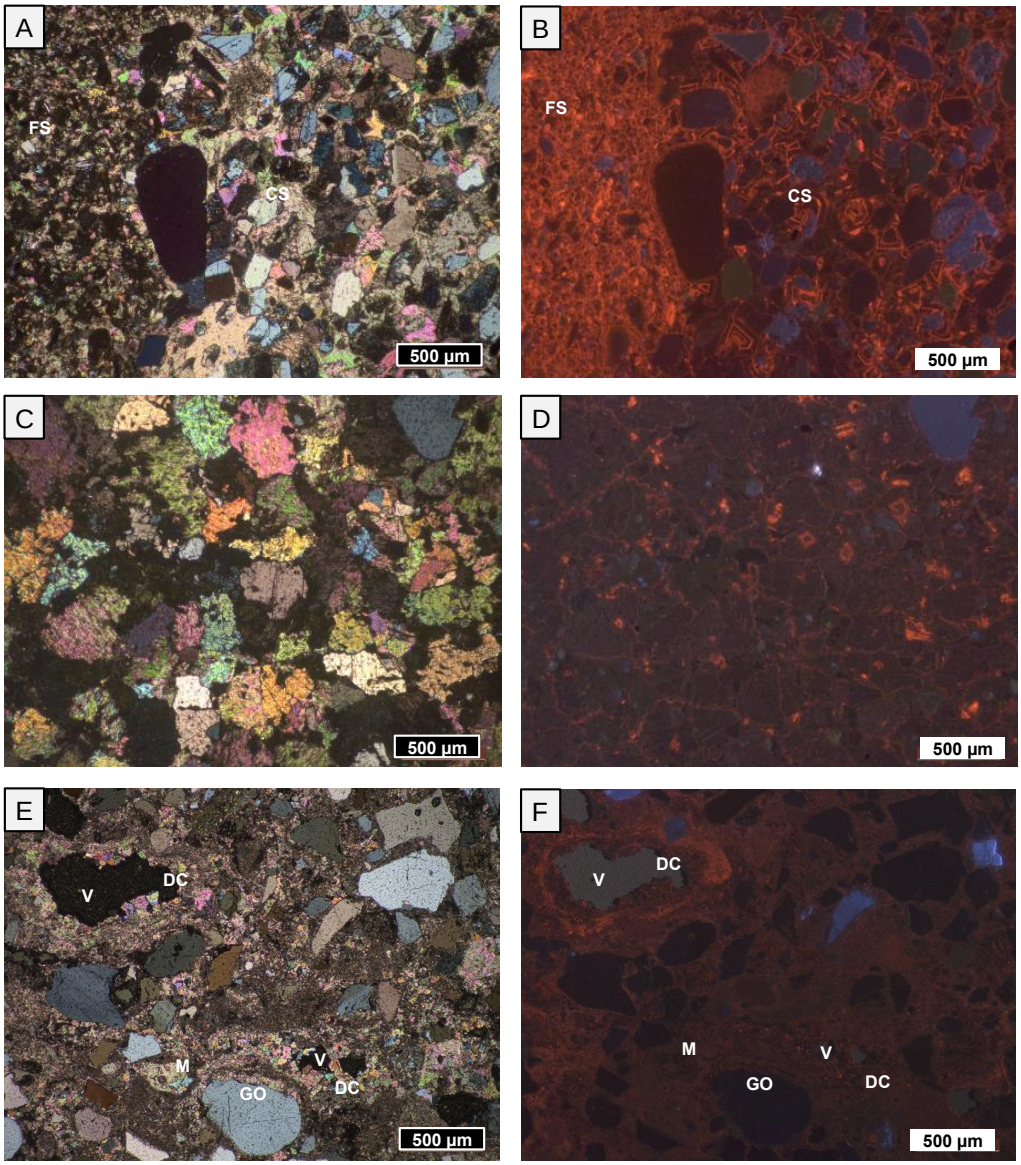

Figure 10: Photomicrographs of carbonate cemented beds. (A) Fine spar (FS) and equant, blocky, sparry calcite (SC) that are 30-200 µm in diameter. Sample is from the Fant tuff subunit of the Catahoula Formation in cross-polarized light. (B) Same picture as A with cathodoluminescence. Sparry calcite of 30-200 µm in diameter displays 2-5 bands of concentric luminescence zonation. (C) Blocky, equant calcite cement ranging from 200-500 µm from the Fant tuff subunit in cross-polarizing light. (D) Same picture as C with cathodoluminesence. Calcite displays only trace amounts of concentric zonation. (E) Two generations of cement consisting of micrite to microsparite (M) rims that coat detrital grains and subsequent coarse drusy calcite (DC) that increases in size toward center of the voids (V). Grain overgrowth in bottom center (GO) by spar calcite is indicated by arcuate boundary along top of the grain. Sample is from the upper portion of the Goliad Formation in cross-polarizing light. (F) Same picture as in E with cathodoluminescence.

granules in the Fant tuff subunit, all have micritic and microsparry carbonate rims (Figure 10E-F). Such carbonate rims only constitute a small proportion of the total pore-filling cement. The cements display variations in luminescence corresponding to their texture. The equant and blocky spars generally contain 2-5 bands of bright orange to dull concentric zonation (Figure 10B, F). The spars greater than 200 μm mostly displays dull luminescence, but faint orange luminescence was observed along crystal contacts (Figure 10D). The microspars and fine spars in fine-grained sandstone have spatially intermixed orange or red luminescence and dull luminescence (Figure 10F). The $\delta^{18}O$ and $\delta^{13}C$ values of subsamples micromilled from areas of variable spar texture and luminescence vary up to 1.3 ‰ and 2.0 ‰, respectively.

These carbonate-cemented beds in south Texas are similar to those described by Mack et al. (2000), Hall et al. (2004), and Alonso-Zarza and Wright (2010). The sharp boundaries that conform to bedding planes, and lack of pedogenic textures suggest groundwater origins of these carbonates (Mack et al, 2000; Alonso-Zarza and Wright, 2010). The point and long contacts and the large intragranular area indicate lack of compaction induced by deep burial, thus the cements were most likely formed during early diagenesis (McBride, 1994). The micrites and microspars present as detrital grain rims were likely formed in vadose zone where water adheres due to higher capillary draw (Palmquist and

Johnson, 1962; Hillel, 1980; Jury et al., 1991), and this process happened most likely very early, before burial of sediment in the phreatic zone, due to high levels of supersaturation and rapid precipitation induced by rapid evaporation and transpiration (Longman, 1980; Mack et al., 2000; Hall et al., 2004). The equant, blocky interstitial spars are typical results of cement precipitation within phreatic zone (Longman, 1980; Mack et al., 2000; Hall et al., 2004). Burial of sediments below the water table promoted formation of drusy and blocky spars in slower precipitation rates due to lower supersaturation of calcite (Longman, 1980; Hall et al., 2004). Dull luminescence of large spars formed in the phreatic zone may be induced by fast carbonate precipitation rate, low Mn concentrations in reduced groundwater, or quenching of luminescence by certain type of rare earth elements (Machel and Burton, 1991). The variations of luminescence in concentric zonation of coarse spars, fine spars, and microspars may suggest frequent changes in precipitation rate or temperature (Machel and Burton, 1991). Variations in $\delta^{18}O$ and $\delta^{13}C$ values within the same cemented bed can be attributed to changes in groundwater isotopic composition, variable amount of evaporation and meteoric input, and carbonate growth temperature at variable depths.

Groundwater carbonate concretions

The least common type of carbonates in south Texas are groundwater concretions. In outcrop, groundwater concretions are only found in tuffaceous, fine-grained sandstone in the Fant tuff subunit of the Catahoula Formation, and

are positioned immediately beneath horizontal root mats (Figure 9D). The concretions are elongated, parallel to bedding planes. They are 1-10 cm in diameter, and 30 cm in length. Most concretions are single, but in some cases, they coalesce into a large mass. Under microscope, the concretions contain interstitial, fine, equant spars in poikilotopic texture (Figure 11D-E). Some of the spars are coarse, up to 2 mm in size. The poikilotopic spars show different degree of luminescence, with predominantly dull luminescence or faint zonation in some samples, and intermixed bright orange and dull luminescence in other samples (Figure 11C, F). The $\delta^{18}O$ and $\delta^{13}C$ values of subsamples corresponding to various spar texture and luminescence range up to 0.8 ‰ and 2.3 ‰, respectively.

The carbonate concretions observed in the Fant tuff subunit in south Texas are similar to the phreatic concretions studied by Mack et al. (2000) and zoned concretions described by Mozley and Davis (2005). The elongation of these concretions along beddings, lack of soil structural elements, and sparry poikilotopic texture all indicate groundwater origin of this type of carbonates (Mack et al, 2000; Hall et al., 2004; Alonso-Zarza and Wright, 2010). The alignment of the concretions may reflect regional groundwater flow directions (McBride et al., 1994; Mozley and Davis, 1996, 2005). The association of concretions with overlying root mats further supports groundwater origin because root mats were probably formed in waterlogged near-surface sandy sediment (Mack et al., 2000; Alonso-Zarza and Wright, 2010). Faint zonation and high

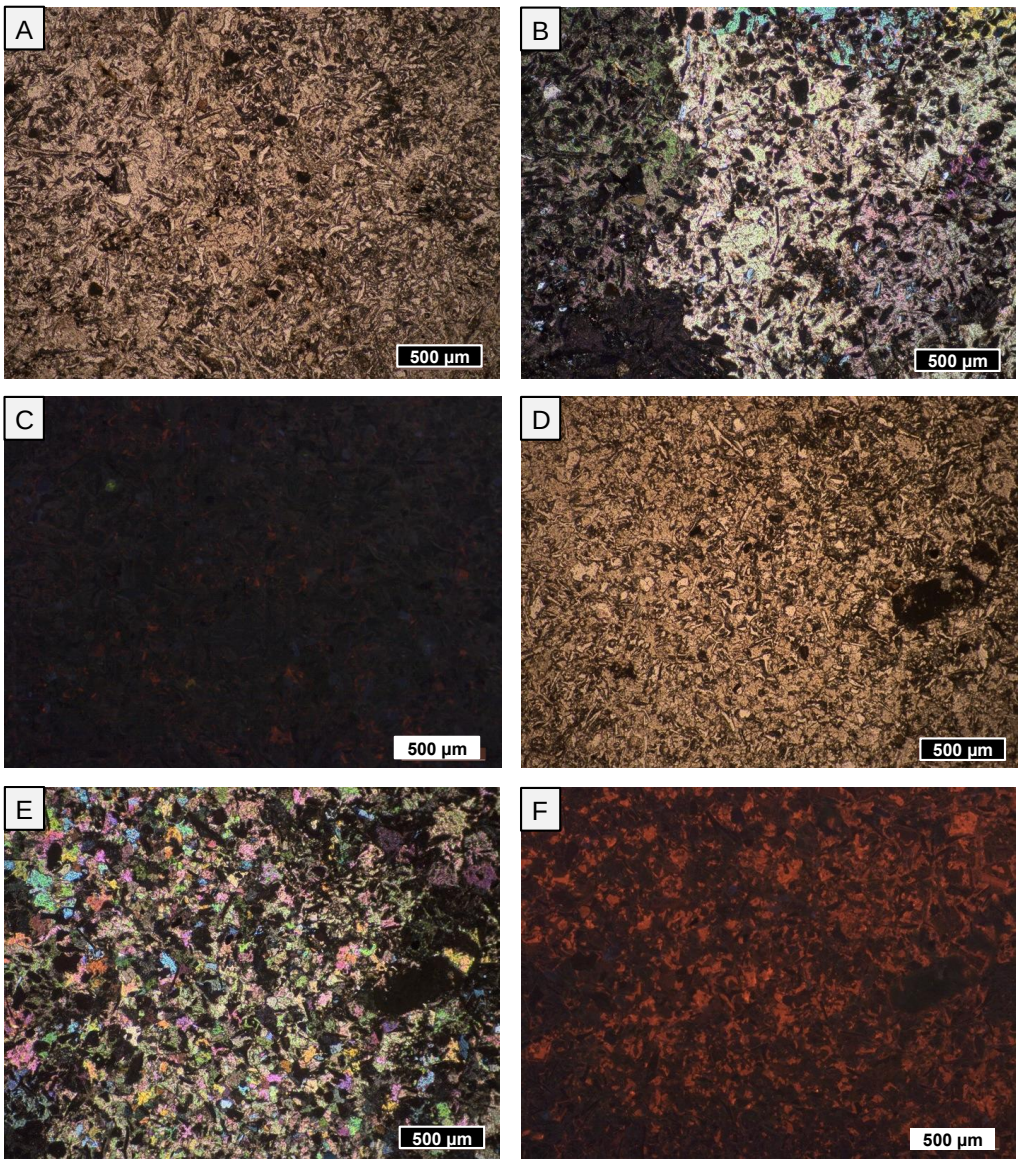

Figure 11: Photomicrographs of groundwater carbonate concretions. (A) Equant, blocky, poikilotopic textured calcite within the Fant tuff subunit of the Catahoula Formation. Irregular, clear, elongated clasts are reworked glass shards in plane-polarized light. (B) Same sample as in A showing spars filling pore spaces in cross-polarized light (C) Same sample as in A with cathodoluminescence. (D) Equant, blocky calcite spars in the Fant tuff subunit in plane-polarized light. (E) Same sample as in D in cross-polarized light. Note fine calcite spar in center, and coarse calcite spar in the upper left corner. (F) Same sample as in D with cathodoluminescence.

abundance of cementation imply concentric growth of the concretions (Mozley and Davis, 2005). Dull luminescence and intermixed bright and dull luminescence in phreatic zone may be induced by temporal fluctuations in carbonate precipitation rate, Mn^{2+} concentrations in groundwater, or quenching of luminescence by certain type of rare earth elements over the course of concretion formation (Machel and Burton, 1991). Variations in the $\delta^{18}O$ and $\delta^{13}C$ values within the same concretion reflect changes in groundwater isotopic compositions, or carbonate growth temperature and depth, which corroborates the interpretation of variable luminescence.

Discussion

The pedogenic carbonates described in this study display texture and luminescence characteristics typical of pedogenic origin within the vadose zone, except for some of the rhizoliths, which may form in the phreatic zone. The groundwater carbonates all display textures characteristic of early diagenetic cement in the shallow subsurface immediately above, at, or below the water table. The studied Oligocene-Miocene strata in south Texas were never deeply buried, thus the samples did not experience deep diagenesis. Significant amounts of diagenesis would tend to homogenize the isotopic composition of carbonates. The isotopic values within the same specimen, same type of carbonates, and same stratigraphic level show variability, suggesting that diagenesis is very minor in the

studied samples. Therefore, the $\delta^{18}O$ and $\delta^{13}C$ values of the studied carbonates reflect paleoclimate and paleoenvironment in south Texas during the Oligocene and Miocene.

1. Isotopic differences among different types of carbonates

Pedogenic carbonates form in equilibrium with soil water, of which precipitation is the principal component (Cerling and Quade, 1993; Breeker et al., 2009; Fox et al., 2012a). Therefore, the $\delta^{18}O$ values of pedogenic carbonates record meteoric water $\delta^{18}O$ values and carbonate precipitation temperature (Cerling and Quade, 1993; Quade and Cerling, 1995; Breecker et al., 2009). Variations in isotopic values within pedogenic carbonates in the same stratigraphic interval are small, up to ~3 ‰ (Figure 12). This range agrees with the range of $\delta^{18}O$ values described for Quaternary pedogenic carbonates in south Texas (Zhou and Chafetz, 2010). The pedogenic carbonate nodules seem to have slightly higher $\delta^{18}O$ values than those of the platy horizons, but are lower than or equal to those of the rhizoliths (Figure 12). Although soil water $\delta^{18}O$ values are influenced by evaporation at shallow depth, typically above 30 cm (Cerling and Quade, 1993; Quade and Cerling, 1995; Breeker et al., 2009), the pedogenic carbonates $\delta^{18}O$ values in soil profiles in this study show very subtle decrease with depth within the Chusa subunit of the Catahoula Formation, and a subtle decrease with depth within the Oakville Formation (Figure 13), suggesting that

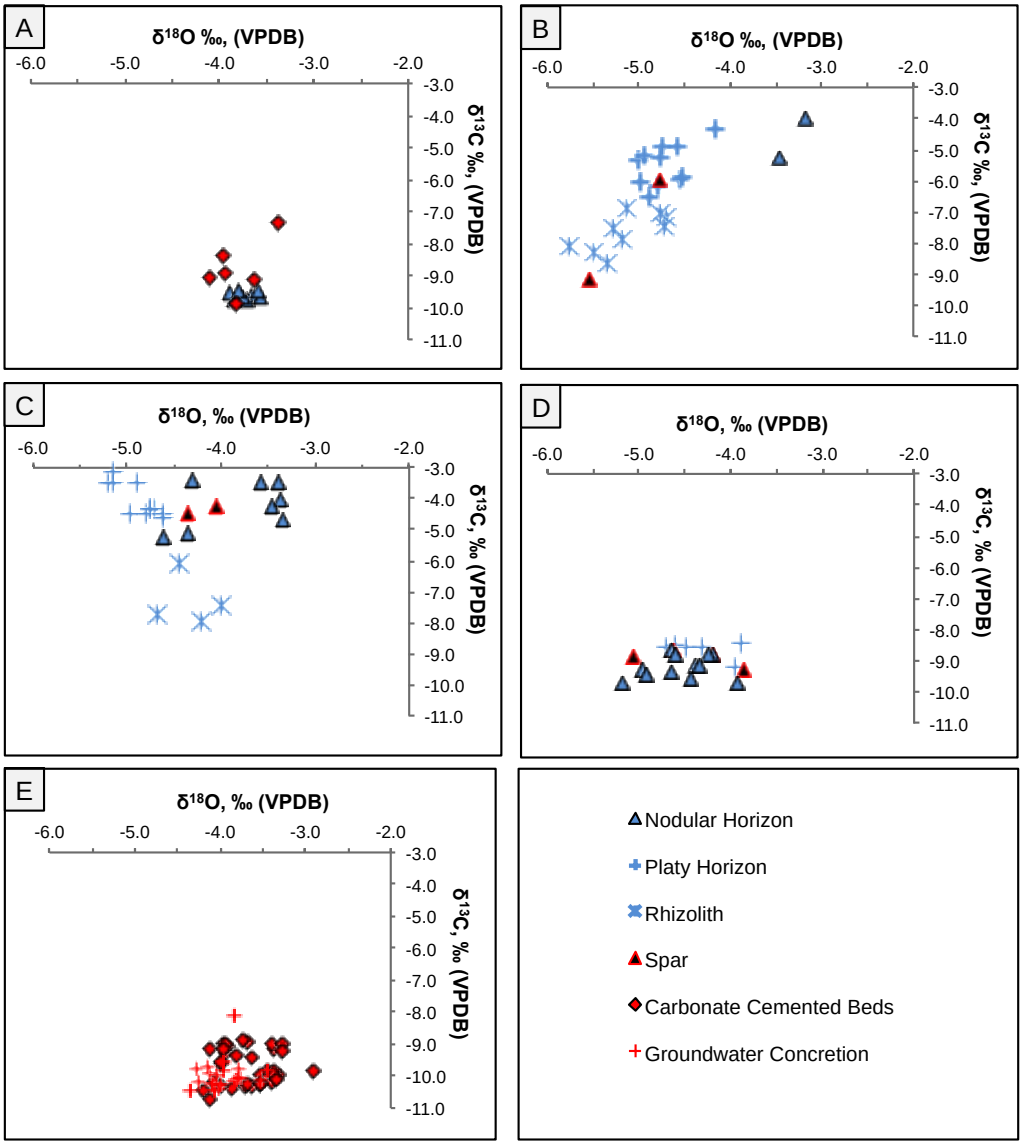

Figure 12: Carbon and oxygen isotope crossplots. Values were reported relative to Vienna Peedee Belemnite (VPDB) for the (A) upper portion of the Goliad Formation; (B) lower portion of the Goliad Formation; (C) Oakville Formation; (D) Chusa subunit of the Catahoula Formation; and (E) Fant tuff subunit of the Catahoula Formation.

the $\delta^{18}O$ values of these carbonates were not significantly influenced by evaporation. Therefore, the subtle differences in the $\delta^{18}O$ values of different

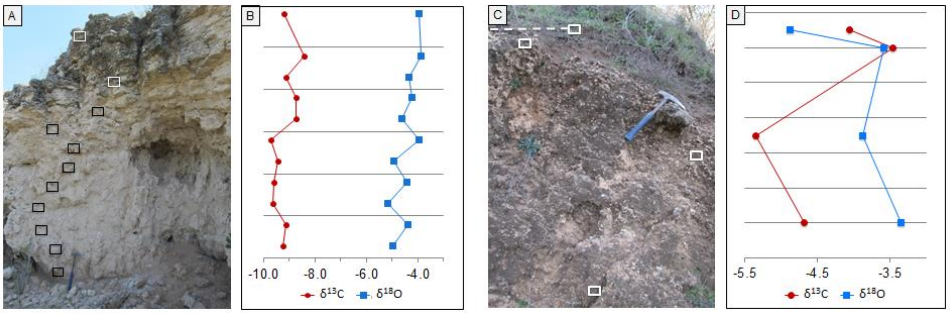

Figure 13: Two pedogenic carbonate profiles in outcrop and isotope compositions. (A) Calcic soil profile within the Chusa subunit of the Catahoula Formation sampled every 25 cm within the nodular horizon (black boxes) and platy horizon (white boxes). (B) Stable isotopic compositions at depth reported relative to VPDB. (C) Nodular horizon within the Oakville Formation sampled every 50 cm (white boxes). (D) Stable isotopic compositions at depth reported relative to VPDB.

types of pedogenic carbonates most likely reflect formation of these carbonates in different time when soil temperature changed or soil water $\delta^{18}O$ values changed between those of mean annual precipitation and summer precipitation (e.g., Breecker et al., 2009). The slightly lower $\delta^{18}O$ values in the rhizoliths than in the pedogenic carbonate nodules may be caused by the addition of groundwater during rhizolith formation because these roots may grow deep, or the bias to summer formation of soil nodules under equilibrium with summer precipitation in the semi-arid climate (e.g., Breecker et al., 2009; Hough et al., 2014).

Groundwater carbonates form typically in equilibrium with shallow groundwater, which is a mixture of local meteoric water and river water that carries the mean isotopic values of precipitation in the river catchment (e.g.,

Quade and Roe, 1999). The lack of systematic difference in the $\delta^{18}O$ values of groundwater carbonates and pedogenic carbonates (Figure 12A) suggest that the groundwater $\delta^{18}O$ values and groundwater carbonates formation temperature are not significantly different from those of pedogenic carbonates, which further suggests that local precipitation is the major source of groundwater (Quade and Roe, 1999; Mack et al., 2000). It is also possible that oxygen isotope fractionation associated with lower carbonate formation temperature in phreatic zones and at lower mean annual precipitation $\delta^{18}O$ values compensate the fractionation associated with higher carbonate formation temperature in soils with warm season precipitation $\delta^{18}O$ values. In either case, the groundwater carbonates and pedogenic carbonates record surface water isotope information and temperature, thus can be used together to discuss climate controls on the carbonates $\delta^{18}O$ values in south Texas through time.

Pedogenic carbonates form in equilibrium with soil CO_2 dissolved within soil water (Cerling, 1984; Cerling et al., 1991). Soil CO_2 is composed of a mixture of atmospheric and soil respired CO_2, with the atmospheric component decreasing with depth until soil respired CO_2 is dominant and the $\delta^{13}C$ value of soil respired CO_2 reflects plant types and water availability (e.g., Cerling et al., 1991; Breecker et al., 2009; Fox et al., 2012). The pedogenic carbonates sampled from the same stratigraphic intervals have $\delta^{13}C$ values ranging up to ~5 ‰ (Figure 12B and 12C), consistent with what has been reported for Quaternary pedogenic

carbonates in south Texas where the vegetation contains ~60% C_3 and ~40% C_4 plants (Zhou and Chafetz, 2010). Some of our rhizoliths have distinctly lower $\delta^{13}C$ values than the nodular and platy horizons in the same stratigraphic intervals (Figure 12). Modern C_3 plants are woody trees and shrubs with root abundance greater than 90 cm in soil profiles, and the $\delta^{13}C$ values are offset from herbaceous C_4 plants with shallow root systems by at least ~ -13 ‰ in south Texas (Boutton, 1998). The $\delta^{13}C$ values of carbonates formed by C_3 plants are typically -12 ‰ and the values of carbonates formed by C_3 plants are typically 2 ‰ (Cerling, 1984; Cerling and Quade, 1993). Because I have sampled some rhizoliths from either below the nodular horizon or in intervals (such as the Flemmings Formation) with little development of soil horizons, they are very likely biased to C_3 shrubs or trees because of the greater depth in formation, and their $\delta^{13}C$ values are mostly influenced by C_3 plant respired CO_2. The carbonates from the platy and nodular horizons are comparable, and show little upward increase in soil profiles (Figure 13), suggesting that the $\delta^{13}C$ values reflect soil respired CO_2, with little influence of atmospheric CO_2. Therefore, the $\delta^{13}C$ values of pedogenic carbonates can be used to discuss ecologic change in south Texas through time.

2. Changes in paleoclimate during the Oligocene and Miocene

The minimum carbonate $\delta^{18}O$ values decreased from -4.3 ‰ during the early Oligocene to -5.8 ‰ during the middle Miocene, and these values are all

higher than the estimated modern groundwater carbonates $\delta^{18}O$ values (Figure 14). By using the mean $\delta^{18}O$ value of the Nueces River water (IAEA, 2017), and a mean annual temperature (MAT) of 22° C in south Texas (Yu et al., 2006), I calculated that modern carbonates formed in equilibrium with groundwater in the study area has a $\delta^{18}O$ value of -6.5 ‰ following the fractionation equation in Kim and O'Neil (1997). This value is slightly lower than the $\delta^{18}O$ values of Quaternary pedogenic carbonates in south Texas (Figure 14) (Zhou and Chafetz, 2010),

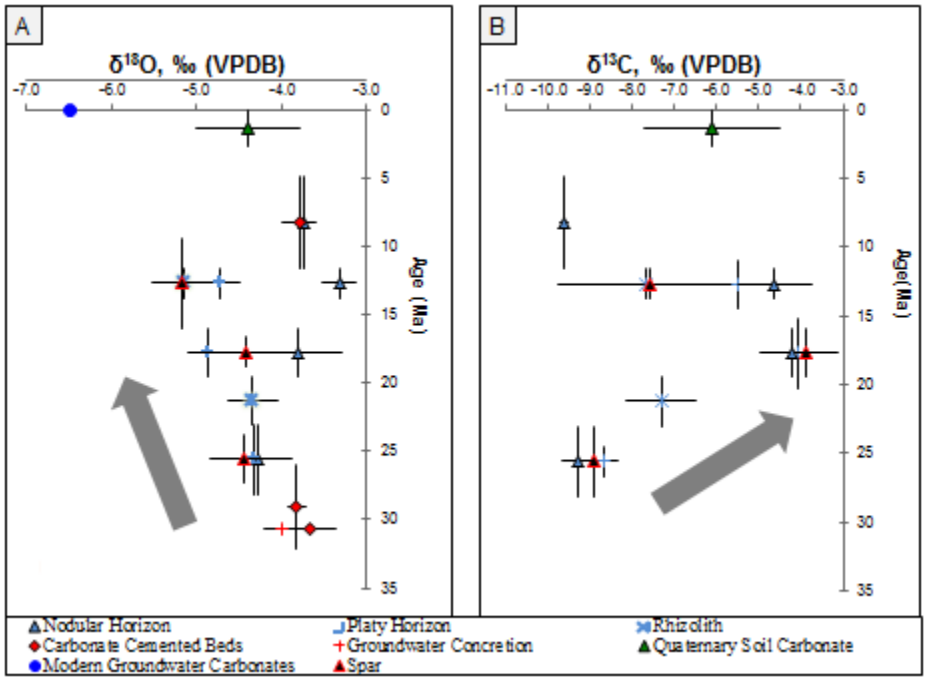

Figure 14: Changes in mean carbonates $\delta^{18}O$ (A) and $\delta^{13}C$ values (B) in south Texas. Errors of isotope data are one standard deviation. Quaternary soil carbonates data are from Zhou and Chafetz (2010). Modern river water data used to calculate $\delta^{18}O$ value of modern groundwater carbonates formed in equilibrium with river water are from the Nueces River in Three Rivers, TX (IAEA, 2017).

which is possibly induced by the formation of pedogenic carbonates in warm seasons. Because the maximum carbonate $\delta^{18}O$ values suggest possible formation

of pedogenic carbonates in warm seasons, I use the minimum carbonate $\delta^{18}O$ to interpret the changes in paleoclimate.

The minimum values of the carbonates $\delta^{18}O$ values decreased ~3 ‰ after the early Oligocene in south Texas. The latitude, continentality, and elevation of the study area did not change since the early Oligocene, and vapor source of the study area should be the Gulf of Mexico during the entire Cenozoic. Therefore, the most likely causes of the decrease in the carbonates $\delta^{18}O$ values is air temperature and seawater $\delta^{18}O$ values. Air temperature influences carbonate $\delta^{18}O$ values by causing changes in precipitation $\delta^{18}O$ values (0.69 ‰/°C, Dansgaard, 1964), and isotope fractionation between water and carbonate (-0.23 ‰/°C, Kim and O'Neil, 1997). The net result of temperature change on carbonate $\delta^{18}O$ is 0.46 ‰/°C. The ~3 ‰ decrease can be explained by 6° C cooling during the Oligocene and Neogene if seawater $\delta^{18}O$ values remained the same. However, seawater $\delta^{18}O$ values have increased because of increase in global ice volume during the Neogene (Emiliani, 1966; Shackleton and Opdyke, 1976). Although it is difficult to know the amount of change in surface seawater $\delta^{18}O$ values, the increase in seawater $\delta^{18}O$ values makes my estimate of 6° C cooling a minimum.

While continental records of cooling after the Oligocene are rare, one study based on clumped isotope paleothermometry suggested that the central Rocky Mountains and the adjacent Great Plains in western U.S. have cooled ~5° C since the early Oligocene (Fan et al., 2014b). The 6 °C cooling documented in

south Texas in this study is comparable to the continental record in Fan et al. (2014b), but is higher than the changes in sea surface temperatures (SST). The reconstructed SST in the Gulf of Mexico during the early Oligocene is 29±2.2 °C based on TEX_{86} analysis (Wade et al., 2012). Modern SST of the region is 26° C (Raynor et al., 2003) indicating a ~3° C drop since the early Oligocene.

3. Changes in paleoenvironment during the Oligocene and Miocene

The minimum pedogenic carbonates $\delta^{13}C$ values increased from -9.7 ‰ during the late Oligocene, to -5.3 ‰ during the middle Miocene (Figure 14B). These values are lower or comparable to the $\delta^{13}C$ values of Quaternary pedogenic carbonates in south Texas (Zhou and Chafetz, 2010). The 4.4 ‰ increase during the early Neogene cannot be explained by addition of more atmospheric CO_2 to our samples through time because our $\delta^{13}C$ values do not show gradual decrease in paleosol profiles (Figure 13), which is indicative of atmospheric input at shallow soil depths (Cerling, 1984; Cerling and Quade, 1993). Carbonate $\delta^{13}C$ values can increase up to ~6.2 ‰ due to decreased fractionation of ^{13}C by C_3 plants in water-stressed environments (Farquhar et al., 1989; Cerling and Harris, 1999; Fessendon and Ehleringer, 2003). Water-stressed conditions are not likely the cause of the 4.4 ‰ increase because our samples do not display positive covariance between $\delta^{13}C$ and $\delta^{18}O$ values, suggesting that the soil water was not

evaporated due to changes in aridity (Fox et al., 2012a). The most likely cause of the gradual increase in $\delta^{13}C$ values is the expansion of C_4 biomass.

Modern Crassulacean acid metabolism (CAM) and C_4 plants mean $\delta^{13}C$ values from south Texas are offset by only ~ 1.5 ‰. By assuming that soil respiration rates were high enough to minimize atmospheric contribution of CO_2, I used the following mass balance equation in Fox and Koch (2004) with measured $\delta^{13}C$ values of modern C_3 and C_4 end members of -26.9 ‰ and -14 ‰, respectively (Boutton, 1998), to calculate the percentage of C_4 and CAM plants.

$$\delta^{13}C_{carbonates} = (1- X)\ \delta^{13}C_{mean\ C3} + (X)\ \delta^{13}C_{mean\ C4}$$

The results show that C_4 and CAM plants increased from ~ 13% during the late Oligocene to ~ 43% during the middle Miocene. Modern C_4 abundance in south Texas is 55 to 65% and CAM plants range from 16 to 38% (Koch et al., 2004), which are greater than my estimates. The estimated C_4 abundance agrees with the estimated 20 to 30% C_4 in the Great Plains during the early Miocene (Fox and Koch, 2003). My documented late Oligocene expansion of C_4 and CAM plants, however, is at least ~16 myr older than the documented expansion at 9.4-7.2 Ma in northern India (Quade and Cerling, 1995; Quade and Roe, 1999). The earlier expansion of C_4 plants in south Texas underscores the need to study how local

climatic factors (Huang et al., 2001) modify and in some cases pre-date global driving mechanisms (Fox and Koch, 2004) in the expansion of C_4 biomass.

Conclusions

Continental carbonates of the Oligocene and Miocene age in south Texas were studied in order to understand the origins of the carbonates and the paleoclimate and paleoenvironment. Field observations and thin section characterizations identify three types of pedogenic carbonates, including rhizoliths, carbonate nodules, and platy horizons, and two types of groundwater carbonates, including cemented beds and carbonate concretions. In outcrop, the pedogenic carbonates display gradational lower and sharp upper contacts, and contain soil structural elements such as nodules and biogenic elements such as rhizoliths. The groundwater carbonates are restricted to permeable units, display sharp lower boundaries and destruction of original beddings, and lack of pedogneic profiles. Under microscope, the pedogenic carbonates are micritic with clotted micrite and alveolar-septal structures and display dull cathodoluminescence, while the groundwater carbonates contain equant, blocky spars, which are occasionally drusy or poikilotopic textured and display concentrically zoned bright orange cathodoluminescence. The preservation of microfabrics and variability of carbon and oxygen stable isotopic compositions at

different scales suggest that these carbonates experienced minimal diagenesis, thus their isotopic compositions reflect paleoclimate and paleoecology in south Texas. The $\delta^{18}O$ values of the continental carbonates decreased ~3 ‰ after the earliest Oligocene, suggesting a minimum of 6° C drop in mean annual temperature in south Texas. The $\delta^{13}C$ values of the pedogenic carbonates increased ~4.4 ‰ from the late Oligocene to the middle Miocene, suggesting an expansion of C_4 plants in south Texas as early as the early Miocene. This early Miocene expansion of C_4 plants is ~16 myr older than what has been documented in Asia, possibly a result of local climate change rather than global climate change.

Appendix A

Stable Isotope Results

Stable carbon and oxygen isotopic values of continental carbonates from south Texas.

Sample ID	Locality	Texture	Form	Type	$\delta^{13}C$	$\delta^{18}O$
UG-770	G1	Bulk	Cement	Groundwater	-7.4	-3.4
UG-460	G1	Bulk	Cement	Groundwater	-9.9	-3.8
UG-690S1	G1	Spar	Cement	Groundwater	-9.0	-3.6
UG-690S2	G1	Spar	Cement	Groundwater	-8.8	-3.7
UG-690S3	G1	Spar	Cement	Groundwater	-9.4	-3.7
UG-690S4	G1	Spar	Cement	Groundwater	-9.0	-4.0
UG-690CS1	G1	Spar	Cement	Groundwater	-9.1	-3.6
UG-690CS3	G1	Spar	Cement	Groundwater	-8.9	-3.9
UG-690CS4	G1	Spar	Cement	Groundwater	-8.4	-4.0
UG-690CS7	G1	Spar	Cement	Groundwater	-9.0	-4.1
MG-140M1	G1	Micrite	Nodule	Pedogenic	-9.6	-3.7
MG-140M2	G1	Micrite	Nodule	Pedogenic	-9.6	-3.8
MG-140M3	G1	Micrite	Nodule	Pedogenic	-9.7	-3.8
MG-140M4	G1	Micrite	Nodule	Pedogenic	-9.8	-3.7
MG-140M5	G1	Micrite	Nodule	Pedogenic	-9.7	-3.6
MG-140M6	G1	Micrite	Nodule	Pedogenic	-9.6	-3.7
MG-140M7	G1	Micrite	Nodule	Pedogenic	-9.6	-3.9
MG-140M8	G1	Micrite	Nodule	Pedogenic	-9.5	-3.6
MG-140M9	G1	Micrite	Nodule	Pedogenic	-9.5	-3.8
LG-560R2	LO1	Micrite	Rhizolith	Pedogenic	-7.2	-4.7
LG-560R3	LO1	Micrite	Rhizolith	Pedogenic	-8.7	-5.4
LG-560R4	LO1	Micrite	Rhizolith	Pedogenic	-7.8	-5.2
LG-560R5	LO1	Micrite	Rhizolith	Pedogenic	-8.3	-5.5
LG-560R6	LO1	Micrite	Rhizolith	Pedogenic	-7.4	-4.7
LG-560R7	LO1	Micrite	Rhizolith	Pedogenic	-8.1	-5.8
LG-560R8	LO1	Micrite	Rhizolith	Pedogenic	-7.0	-4.8
LG-560R9	LO1	Micrite	Rhizolith	Pedogenic	-7.5	-5.3
LG-560R10	LO1	Micrite	Rhizolith	Pedogenic	-6.9	-5.1
LG-220	LO1	Bulk	Nodule	Pedogenic	-4.0	-3.2
ULG-240AV1	B1	Micrite	Platy	Pedogenic	-4.9	-4.6
ULG-240AV2	B1	Micrite	Platy	Pedogenic	-5.3	-5.0
ULG-240AV3	B1	Micrite	Platy	Pedogenic	-4.9	-4.7
ULG-240AV4	B1	Micrite	Platy	Pedogenic	-6.0	-4.6
ULG-240AV5	B1	Micrite	Platy	Pedogenic	-6.5	-4.9
ULG-240AV6	B1	Micrite	Platy	Pedogenic	-5.2	-4.9
ULG-240AV7	B1	Micrite	Platy	Pedogenic	-5.2	-4.8
ULG-240AV8	B1	Micrite	Platy	Pedogenic	-5.9	-4.5
ULG-240AV9	B1	Micrite	Platy	Pedogenic	-6.1	-5.0
ULG-240AV10	B1	Micrite	Platy	Pedogenic	-6.1	-4.8
ULG-240AV11	B1	Micrite	Platy	Pedogenic	-4.3	-4.2

ULG-40	B1	Bulk	Cement	Groundwater	-6.0	-4.8
ULG-40S	B1	Spar	Cement	Groundwater	-9.1	-5.6
UO-225	K1	Bulk	Platy	Pedogenic	-4.3	-4.8
UO-225D1	K1	Micrite	Platy	Pedogenic	-3.1	-5.2
UO-225D2	K1	Micrite	Platy	Pedogenic	-3.5	-5.2
UO-225D3	K1	Micrite	Platy	Pedogenic	-4.5	-5.0
UO-225D4	K1	Micrite	Platy	Pedogenic	-4.4	-4.8
UO-225D5	K1	Micrite	Platy	Pedogenic	-4.4	-4.7
UO-225AV1	K1	Micrite	Platy	Pedogenic	-3.5	-4.9
UO-225AV2	K1	Micrite	Platy	Pedogenic	-3.5	-5.2
UO-225AV3	K1	Micrite	Platy	Pedogenic	-4.4	-4.8
UO-225AV4	K1	Micrite	Platy	Pedogenic	-4.5	-4.6
UO-225AV5	K1	Micrite	Platy	Pedogenic	-4.6	-4.6
UO-220	K1	Bulk	Nodule	Pedogenic	-3.4	-3.6
UO-170M1	K1	Micrite	Nodule	Pedogenic	-4.1	-3.4
UO-170M3	K1	Micrite	Nodule	Pedogenic	-4.3	-3.5
UO-170M4	K1	Micrite	Nodule	Pedogenic	-3.5	-3.4
UO-170M5	K1	Micrite	Nodule	Pedogenic	-10.0	-4.2
UO-170M6	K1	Micrite	Nodule	Pedogenic	-9.9	-4.1
UO-170M2	K1	Micrite	Nodule	Pedogenic	-5.1	-4.4
UO-170M8	K1	Micrite	Nodule	Pedogenic	-3.4	-4.3
UO-170S1	K1	Microspar	Cement	Groundwater	-4.2	-4.1
UO-170S3	K1	Microspar	Cement	Groundwater	-3.0	-4.8
UO-170S4	K1	Microspar	Cement	Groundwater	-4.4	-4.4
UO-120	K1	Bulk	Nodule	Pedogenic	-4.7	-3.4
LO-210	LO2	Bulk	Rhizolith	Pedogenic	-6.1	-4.5
LO-180	LO2	Bulk	Rhizolith	Pedogenic	-7.4	-4.0
LO-80	LO2	Bulk	Rhizolith	Pedogenic	-7.7	-4.7
LO-150	LO2	Bulk	Rhizolith	Pedogenic	-7.9	-4.2
C-1470	D1	Bulk	Nodule	Pedogenic	-8.8	-4.2
C-1336	D1	Bulk	Platy	Pedogenic	-9.2	-4.0
C-1311M1	D1	Micrite	Platy	Pedogenic	-8.6	-4.5
C-1311M3	D1	Micrite	Platy	Pedogenic	-8.5	-4.6
C-1311M4	D1	Micrite	Platy	Pedogenic	-8.6	-4.3
C-1311S	D1	Spar	Cement	Groundwater	-8.7	-4.2
C-1285	D1	Bulk	Platy	Pedogenic	-8.4	-3.9
C-1260	D1	Bulk	Nodule	Pedogenic	-9.1	-4.3
C-1235	D1	Bulk	Nodule	Pedogenic	-8.8	-4.2
C-1210	D1	Bulk	Nodule	Pedogenic	-8.8	-4.6
C-1210S	D1	Spar	Cement	Groundwater	-9.3	-3.9
C-1185	D1	Bulk	Nodule	Pedogenic	-9.7	-3.9
C-1160	D1	Bulk	Nodule	Pedogenic	-9.4	-4.9
C-1135	D1	Bulk	Nodule	Pedogenic	-9.6	-4.4

C-1135S	D1	Spar	Cement	Groundwater	-8.8	-5.1
C-1110	D1	Bulk	Nodule	Pedogenic	-9.7	-5.2
C-1085	D1	Bulk	Nodule	Pedogenic	-9.1	-4.4
C-1060	D1	Bulk	Nodule	Pedogenic	-9.3	-5.0
C-1060S	D1	Spar	Cement	Groundwater	-8.6	-4.6
C2-150	D1	Bulk	Nodule	Pedogenic	-8.3	-4.1
C2-100M1	D1	Micrite	Nodule	Pedogenic	-9.4	-4.0
C2-100M2	D1	Micrite	Nodule	Pedogenic	-9.4	-3.9
C2-100M3	D1	Micrite	Nodule	Pedogenic	-9.5	-4.1
C2-100M4	D1	Micrite	Nodule	Pedogenic	-9.4	-3.9
C2-100M5	D1	Micrite	Nodule	Pedogenic	-9.5	-3.8
C2-100M6	D1	Micrite	Nodule	Pedogenic	-9.7	-4.0
C2-100M7	D1	Micrite	Nodule	Pedogenic	-9.5	-3.9
C2-100M8	D1	Micrite	Nodule	Pedogenic	-9.4	-3.9
C2-100M9	D1	Micrite	Nodule	Pedogenic	-9.5	-3.9
S-190	D2	Spar	Cement	Groundwater	-7.2	-3.9
S-100	D2	Spar	Cement	Groundwater	-7.0	-3.7
F-360S1	LO3	Spar	Cement	Groundwater	-9.6	-4.0
F-360S2	LO3	Spar	Cement	Groundwater	-9.0	-3.9
F-360S3	LO3	Spar	Cement	Groundwater	-9.1	-4.0
F-360S4	LO3	Spar	Cement	Groundwater	-9.6	-4.0
F-360S5	LO3	Spar	Cement	Groundwater	-9.4	-3.6
F-360S6	LO3	Spar	Cement	Groundwater	-9.2	-3.3
F-360FS1	LO3	Spar	Cement	Groundwater	-9.3	-3.9
F-360FS2	LO3	Spar	Cement	Groundwater	-9.2	-3.4
F-360FS3	LO3	Spar	Cement	Groundwater	-9.0	-3.4
F-360FS4	LO3	Spar	Cement	Groundwater	-8.9	-3.7
F-360FS5	LO3	Spar	Cement	Groundwater	-9.0	-3.3
F-360MS1	LO3	Spar	Cement	Groundwater	-8.9	-3.7
F-360MS2	LO3	Spar	Cement	Groundwater	-9.0	-4.0
F-360MS3	LO3	Spar	Cement	Groundwater	-9.1	-3.9
F-360MS4	LO3	Spar	Cement	Groundwater	-9.1	-4.1
F-360MS5	LO3	Spar	Cement	Groundwater	-9.4	-3.8
F-330FS1	LO3	Spar	Cement	Groundwater	-9.9	-3.5
F-330FS2	LO3	Spar	Cement	Groundwater	-9.9	-3.3
F-330FS3	LO3	Spar	Cement	Groundwater	-10.0	-3.5
F-330FS4	LO3	Spar	Cement	Groundwater	-9.9	-3.5
F-330FS5	LO3	Spar	Cement	Groundwater	-9.8	-3.4
F-330MS1	LO3	Spar	Cement	Groundwater	-10.4	-3.9
F-330MS2	LO3	Spar	Cement	Groundwater	-10.1	-3.5
F-330MS3	LO3	Spar	Cement	Groundwater	-10.2	-3.5
F-330MS4	LO3	Spar	Cement	Groundwater	-10.3	-3.7
F-330MS5	LO3	Spar	Cement	Groundwater	-10.3	-3.6

F-330FS6	LO3	Spar	Cement	Groundwater	-10.2	-3.4
F-330FS7	LO3	Spar	Cement	Groundwater	-10.2	-3.7
F-330FS8	LO3	Spar	Cement	Groundwater	-10.0	-3.4
F-330FS9	LO3	Spar	Cement	Groundwater	-10.1	-3.4
F-330FS10	LO3	Spar	Cement	Groundwater	-10.2	-3.5
F-330S1	LO3	Spar	Cement	Groundwater	-10.2	-4.1
F-330S3	LO3	Spar	Cement	Groundwater	-10.3	-4.0
F-330S4	LO3	Spar	Cement	Groundwater	-10.5	-4.2
F-330S5	LO3	Spar	Cement	Groundwater	-10.7	-4.1
F-330	LO3	Bulk	Cement	Groundwater	-9.8	-2.9
F-130R	LO3	Bulk	Rhizolith	Groundwater	-10.1	-3.5
F-120S1	LO3	Spar	Concretion	Groundwater	-9.8	-4.3
F-120S2	LO3	Spar	Concretion	Groundwater	-9.6	-4.0
F-120S4	LO3	Spar	Concretion	Groundwater	-10.2	-4.2
F-120S5	LO3	Spar	Concretion	Groundwater	-9.8	-4.0
F-120S6	LO3	Spar	Concretion	Groundwater	-10.4	-4.3
F-120S7	LO3	Spar	Concretion	Groundwater	-10.4	-4.0
F-120S8	LO3	Spar	Concretion	Groundwater	-10.4	-4.1
F-120S9	LO3	Spar	Concretion	Groundwater	-10.3	-4.1
F-120S10	LO3	Spar	Concretion	Groundwater	-9.9	-4.1
F-120FS1	LO3	Spar	Concretion	Groundwater	-10.2	-3.8
F-120FS3	LO3	Spar	Concretion	Groundwater	-10.1	-3.8
F-120FS4	LO3	Spar	Concretion	Groundwater	-9.8	-3.5
F-120FS5	LO3	Spar	Concretion	Groundwater	-10.0	-3.8
F-120MS1	LO3	Spar	Concretion	Groundwater	-10.2	-4.0
F-120MS2	LO3	Spar	Concretion	Groundwater	-9.7	-4.1
F-120MS3	LO3	Spar	Concretion	Groundwater	-10.0	-4.0
F-120MS4	LO3	Spar	Concretion	Groundwater	-9.8	-3.8
F-120MS5	LO3	Spar	Concretion	Groundwater	-10.0	-3.8
F-120C	LO3	Bulk	Concretion	Groundwater	-8.1	-3.8

Appendix B

Measured Sections

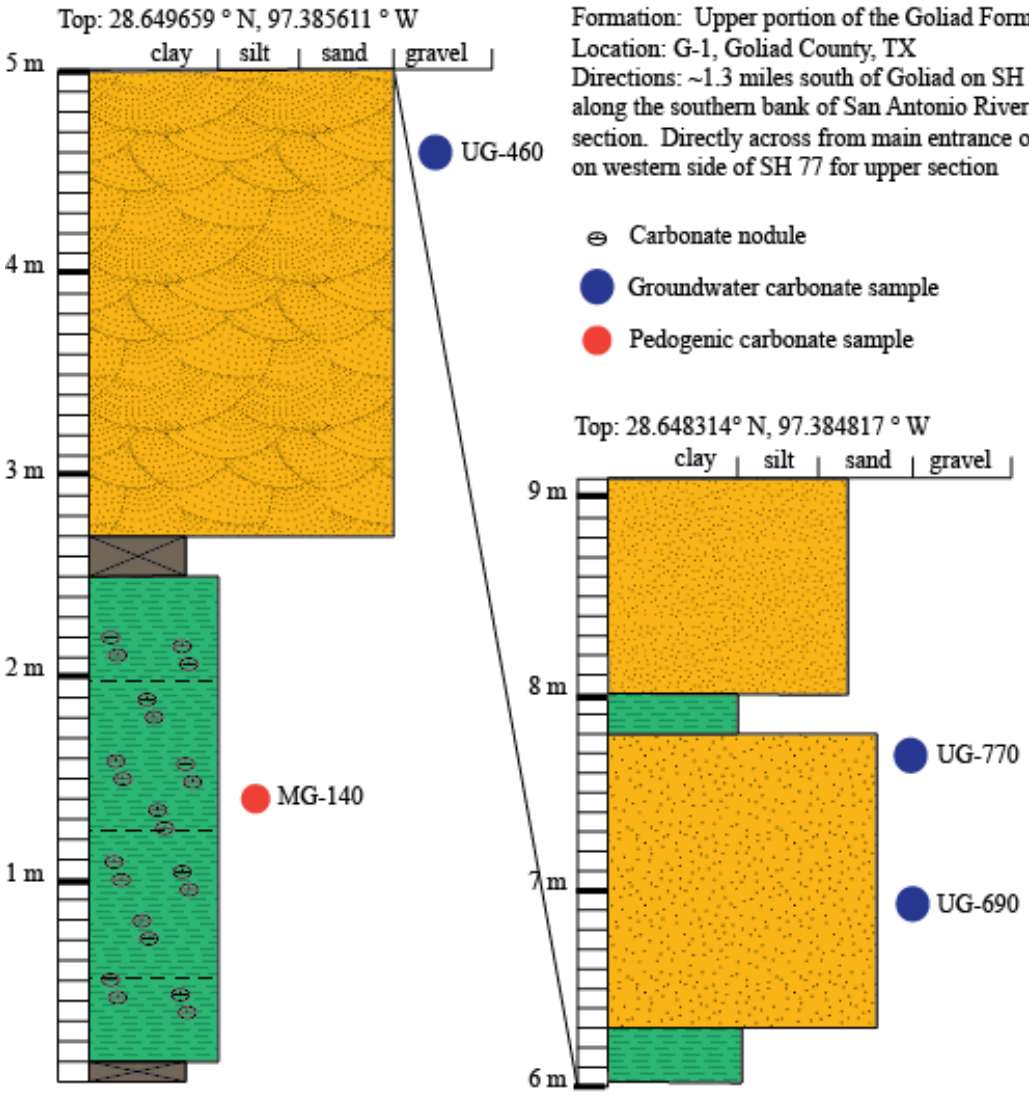

Measured Section
(8.0 - 9.1 m) Medium-grained sandstone, massive
(7.7 - 8.0 m) Clay, massive, white
(6.3 - 7.8 m) Medium to coarse-grained sandstone, massive with discreet packages containing re-worked carbonate nodules
(6.0 -6.3 m) Clay, vertically jointed, white
(5.0 - 6.0 m) Covered
(2.7 - 5.0 m) Pebble conglomeratic sandstone, crossbedded with re-worked carbonated nodules
(2.5 - 2.7 m) Covered
(0.1 - 2.5 m) Sandy clay, massive with abundant carbonate nodules 1-5 cm diameter
(0.0 - 0.0 m) Covered

Formation: Lower portion of the Goliad Formation
Location: B-1, 28.344251 ° N, 97.854675 ° W, Bee County, TX
Directions: ~11 miles east from I-35 on SH 59, roadcut on south side of road

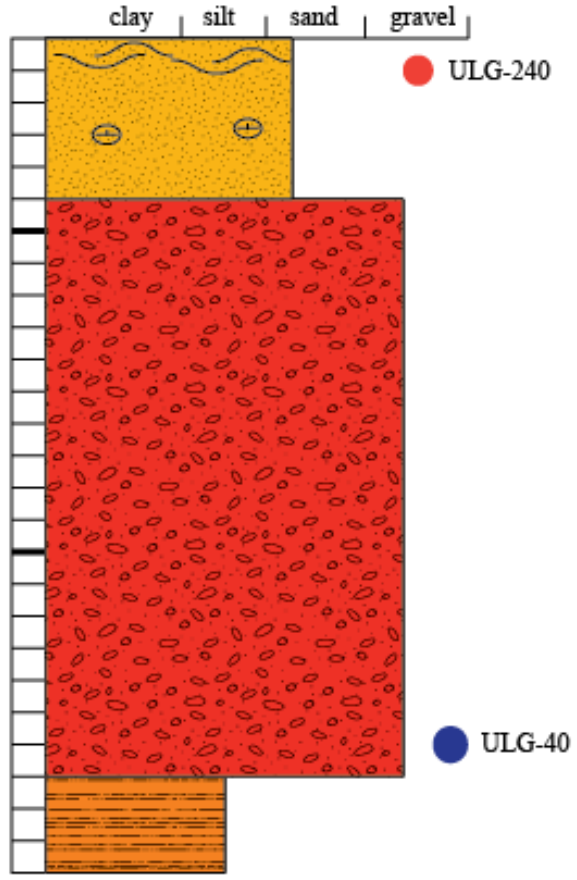

Measured Section
(2.1 - 2.4 m) Fine-grained sandstone, massive, with increasing carbonate content upwards, occasional carbonate nodules near base
(0.3 - 2.1 m) Pebble conglomerate, poorly sorted, laterally variable
(0.0 - 0.3 m) Siltstone, clay-rich


Platy horizon


Carbonate nodule


Groundwater carbonate sample


Pedogenic sample

Formation: Lower portion of the Goliad Formation
Location: LO-1, 28.29411°N, 97.96977 °W, Live Oak County, TX
Directions: I-37 northbound access road, near mile marker 51

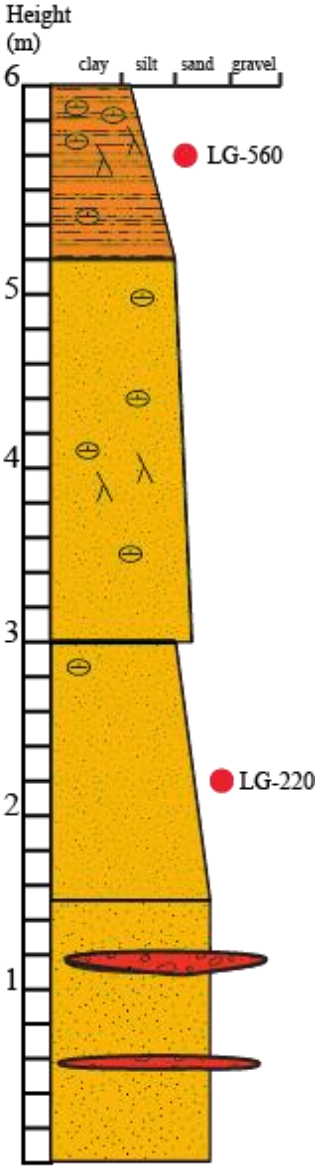

Measured Section

N

(5.2 - 6.0 m) Siltstone and very fine-grained sandstone, abundant carbonate nodules coalesced and abundant root traces at top of exposure

(3.5 - 5.2 m) Fine-grained sandstone, carbonate nodule increase in abundance and degree of induration upwards

(1.5 - 3.5 m) Fine- to medium-grained sandstone, poorly sorted, semi-sonsolidated, contain diffuse carbonate nodules and root traces at the top

(0.0 - 1.5 m) Sandstone contains isolated conglomerate lenses, poorly sorted, gravels are composed of chert, quartz, and re-worked mud clasts

Rhizolith

Carbonate nodule

Pedogenic carbonate sample

Formation: Upper portion of the Oakville Formation
Location: K-1, 28.80357 ^{O}N, -97.79848 ^{O}W, Karnes county, TX
Directions: 1.25 miles south on route 239 from the junction with SH 72 in Kenedy, turn left on gravel road
Outcrop is on right ~300 yards from the road

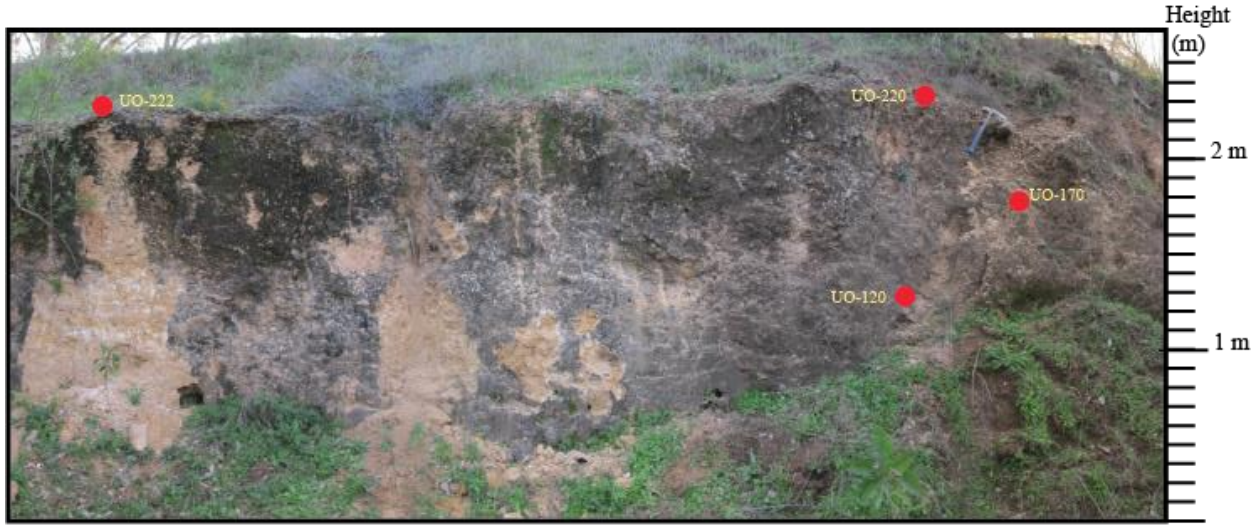

Measured Section
(2.22 m) Platy horizon present at some portions of the outcrop
(1.0 - 2.2 m) Very fine-grained sandstone, fine upwards, massive, carbonate nodules increase in abundance and degree of induration upwards, forming a coalesced nodule horizon in portions of the outcrop
(0.5 - 1.0 m) Fine-grained sandstone, calcareous and massive
(0.0 - 0.5 m) Covered

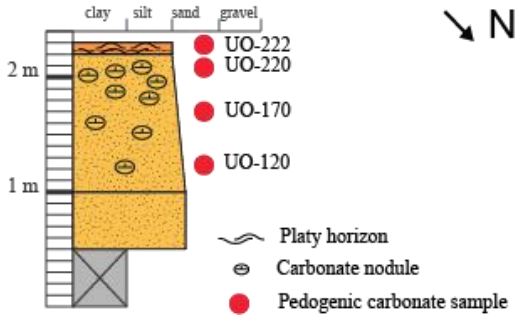

Formation: Lower portion of the Oakville Formation
Location: LO-2, 28.49556 ° N, 98.09591 ° W, Live Oak county, TX
Directions: 2 miles south of Ray Point on the east-west leg of CR 207.

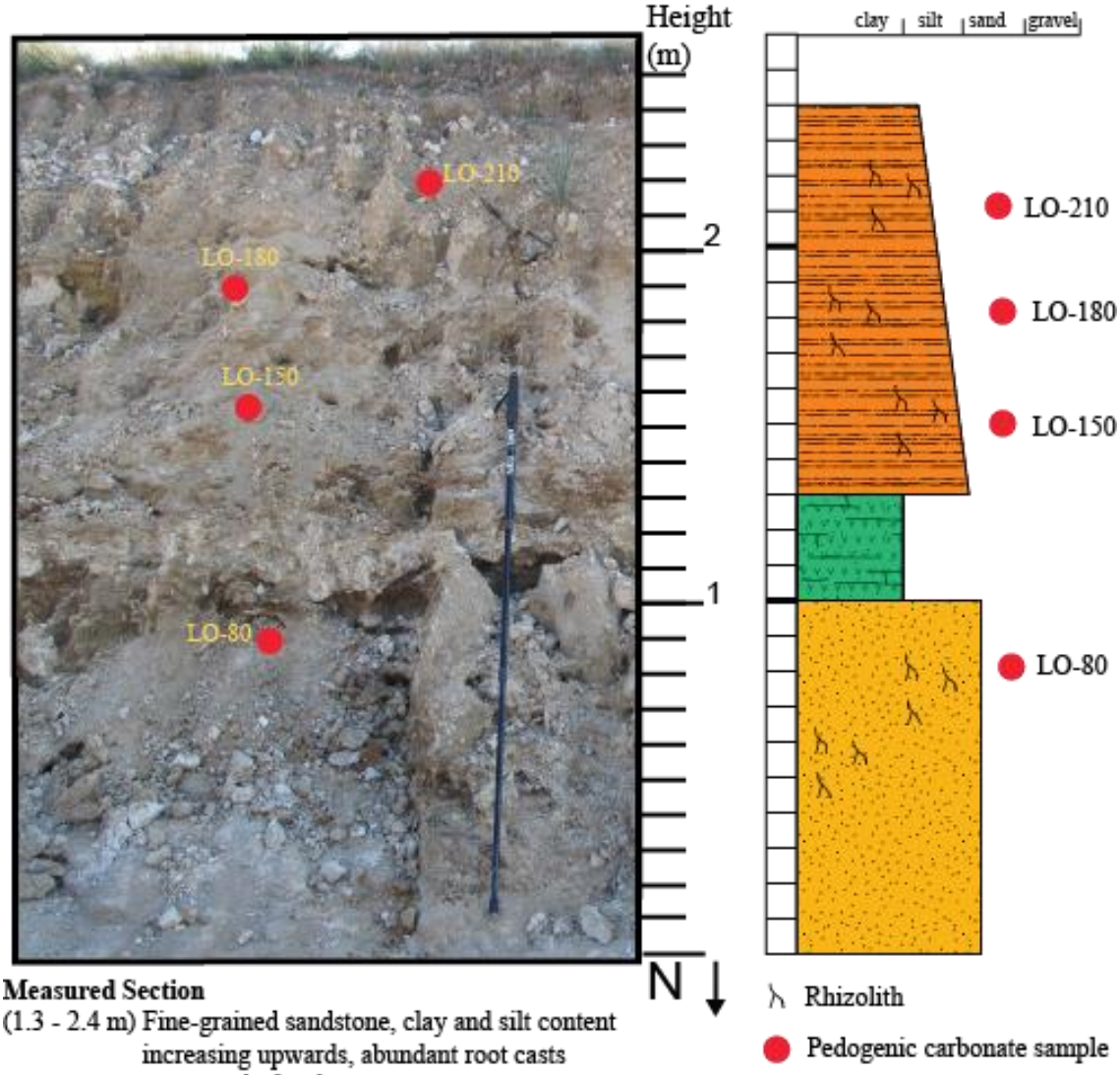

Measured Section

(1.3 - 2.4 m) Fine-grained sandstone, clay and silt content increasing upwards, abundant root casts composed of carbonate

(1.0 - 1.3 m) Ash, re-worked, mud clasts present

(0.0 - 1.0 m) Medium-grained sandstone, massive, mottled brown and yellow, abundant root casts composed of carbonate

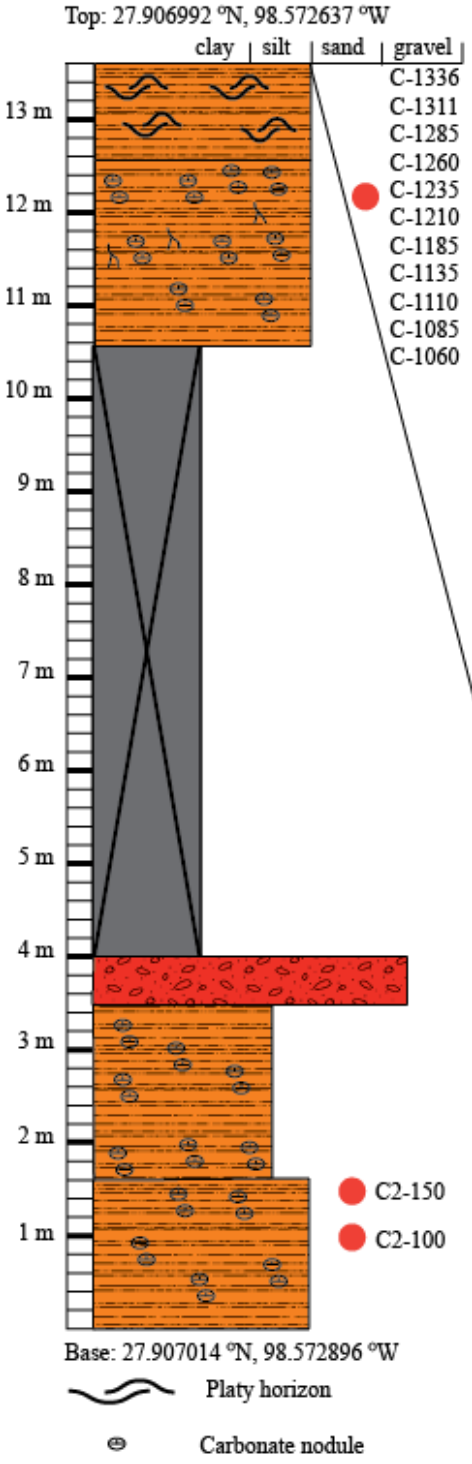

Formation: Chusa subunit of the Catahoula Formation
Location: D-1, Duval County, TX
Directions: ~2 mi northeast of Freer on SH 59.
~300 yards from road to southeast.

Measured Section

(16.8 - 18.6 m) Pebble conglomerate, no grading, crude stratification, composed of limestone, chert, volcanic clasts

(16.6 -16.8 m) Siltstone and very fine-grained sandstone, high clay content, mottled green locally, some ped developement with clay cutans

(15.1 - 16.6 m) Covered

(13.8 - 15.1 m) Siltstone and very fine-grained sandstone, massive, pedogenic carbonate nodules weathered and exposed *in-situ*

(12.6 - 13.8 m) Siltstone and very fine-grained sandstone, massive, high degree of induration, forms cliffs

(10.6 - 12.6 m) Siltstone and very fine-grained sandstone, massive, abundant carbonate nodules elongated vertically with associated root tubules

(4.0 - 10.6 m) Covered

(3.5 - 4.0 m) Pebbel conglomerate lenses, lacking lateral continuity, poorly sorted, matrix supported composed of limestone, chert, volcanic clasts

(1.6 - 3.5 m) siltstone with mud granules, massive, abundant carbonate nodules

(0.0 - 1.6 m) siltstone and very fine-grained sandstone, massive, abundant vertically elongated carbonate nodules

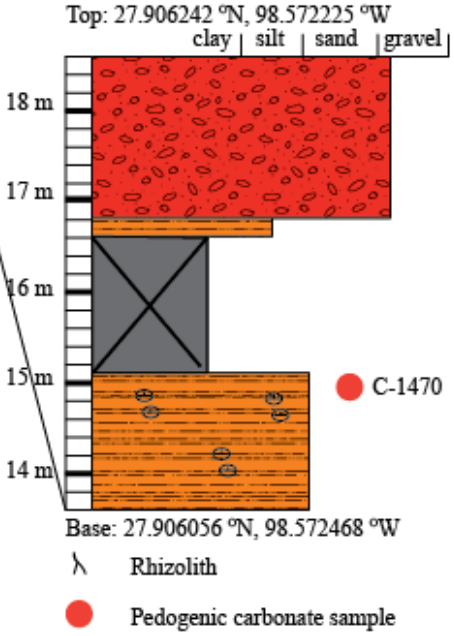

Formation: Soledad subunit of the Catahoula Formation
Location: D-2, Top: 27.863361 ° N, 98.693597 ° W, Duval County, TX
Directions: ~1.5 miles southwest SH44 on SH 59, roadcut north side of road

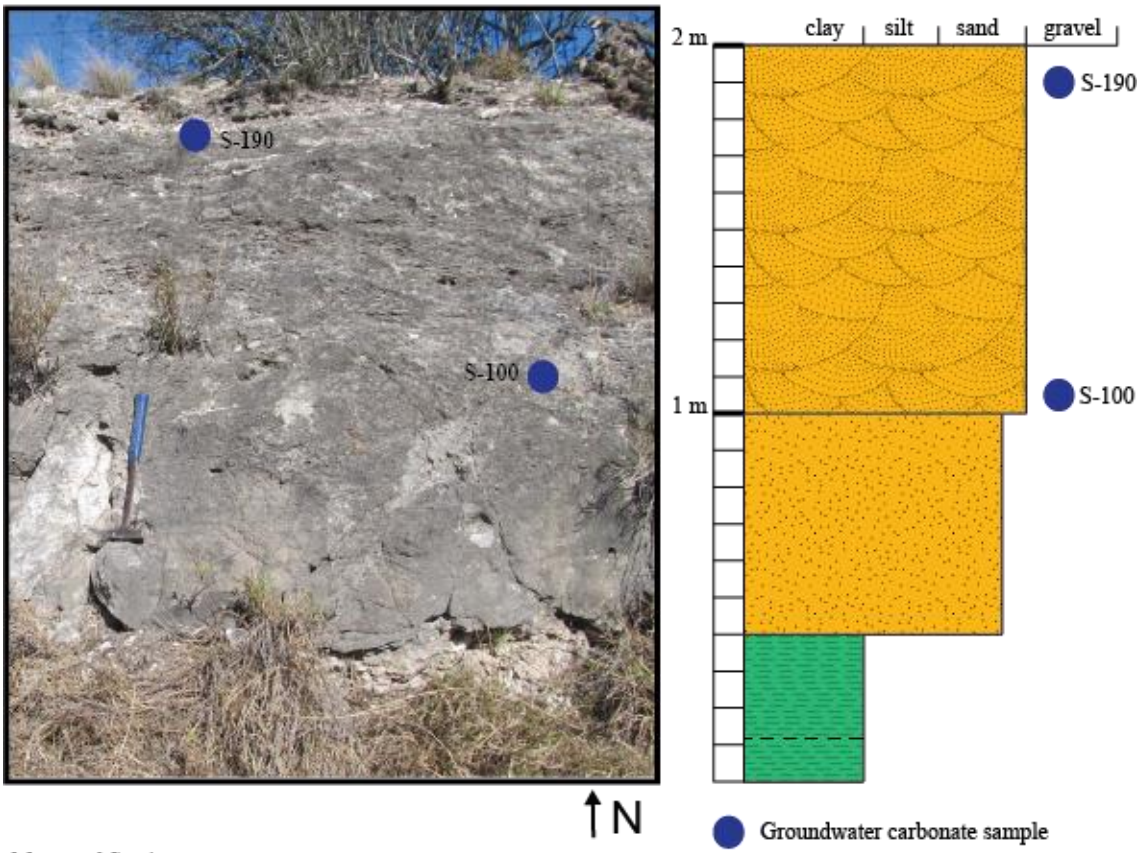

Measured Section
(1.0 - 2.0 m) Conglomeratic coarse-grained sandstone, calcareous, crossbedded, 10-30 cm thick packages amalgamated
(0.4 - 1.0 m) Coarse-grained sandstone, massive, non-calcareous
(0.0 - 0.4 m) Mud clasts with conchoidal fracture

Formation: Fant subunit of the Cathoula Formation
Location: LO-3, Live Oak County, TX
Directions: South shore of Choke Canyon reservoir, adjacent to boat ramp in state park

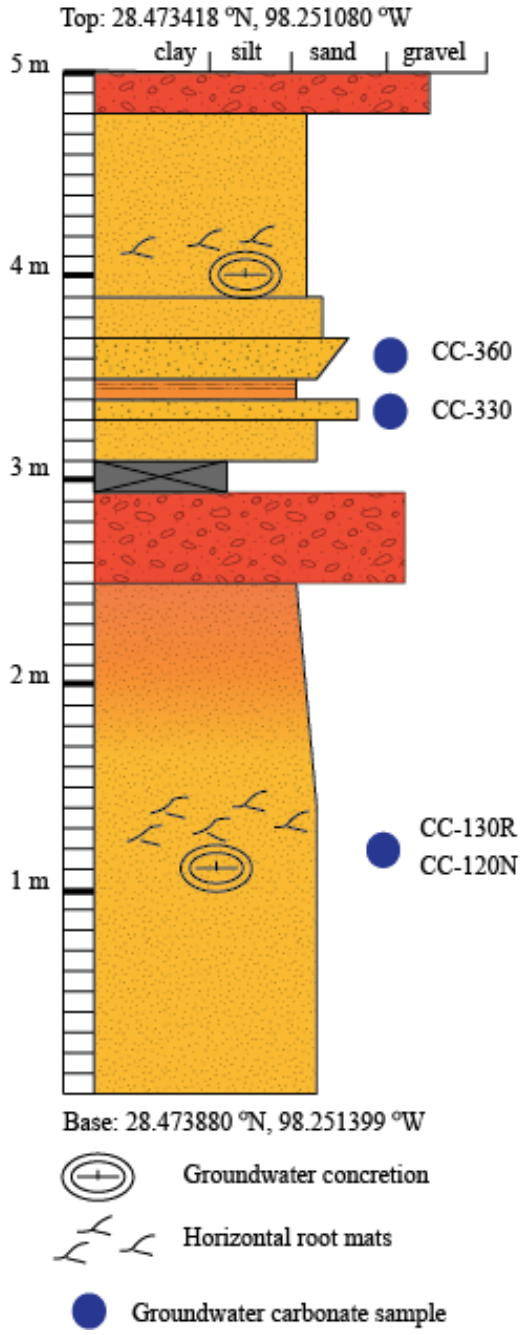

Measured Section

(4.8 - 5.0 m) Granule to cobble conglomerate with clay to coarse sand matrix, poorly sorted, matrix supported, non-imbricated

(3.9 - 4.8 m) Very fine-grained sandstone, massive with occasional concretions 3-9 cm diameter, horizontal root mats at base

(3.7 - 3.9 m) Fine-grained sandstone, massive

(3.5 - 3.7 m) Fine to coarse-grained sandstone, coarsening upward

(3.4 - 3.5 m) Siltstone, massive

(3.3 - 3.4 m) Coarse-grained sandstone, massive

(3.1 - 3.3 m) Very fine-grained sandstone, massive

(2.95 - 3.1 m) Covered

(2.5 - 2.95 m) Pebble to cobble conglomerate with clay to fine sand matrix, poorly sorted, matrix supported, no grading

(1.5 - 2.5 m) Siltstone, massive with decreasing sand content upward

(0.0 - 1.5 m) Very fine-grained sandstone, massive with horizontal root mats and concretions 5-15 cm diameter

References

Alonso-Zarza, A.M., 1999, Initial stages of laminar calcrete formation by roots: examples from the Neogene of central Spain: Sedimentary Geology, v. 126, p. 177-191.

Alonso-Zarza, A.M., and Wright, V.P., 2010, Calcretes, *in*, Alonso-Zarza, A.M., Tanner, L.H., eds., Carbonates in Continental Settings: Facies, Environments, and Processes: Amsterdam, Netherlands, Developments in Sedimentology, v. 61, p. 225-267.

An, Z., Kutzbach, J.E., Prell, W.L., and Porter, S.C., 2001, Evolution of Asian monsoons and phased uplift of the Himalaya-Tibetan plateau since Late Miocene times.: Nature, v. 411, p. 62–66.

Baily, T.L., 1926, The Gueydan, a new middle tertiary formation from the southwestern coastal plain of Texas: Bureau of Economic Geology, University of Texas Bulletin No. 2645, 179 p.

Bain, R.J., and Foos, A.M., 2012, Carbonate microfabrics related to subaerial exposure and paleosol formation, *in*, Carbonate Microfabrics: Springer-Verlag, Frontiers in Sedimentary Geology, p. 19-27.

Baskin, J.A., and Hulbert, R.C. Jr., 2008, Revised biostratigraphy of the middle Miocene to earliest Pliocene Goliad Formation of south Texas: Gulf Coast Association of Geological Societies Transactions, v. 58, p. 93-101.

Beckner, J.R., and Mozley, P.S., 1998, Origin and spatial distribution of early

vadose and phreatic calcite cements in the Zia Formation, Albuquerque Basin, New Mexico, USA, *in*, Morad, S., ed., Carbonate Cementation in Sandstones: Oxford, UK, Blackwell Science, IAS Special Publication, n. 26, p. 27-52.

Boutton, T.W., Archer, S.R., Midwood, A.J., Zitzer, S.F., and Bol, R.,1998, $\delta^{13}C$ values of soil organic carbon and their use in documenting vegetation change in a subtropical savanna ecosystem: Geoderma, v. 82, p. 5 –41.

Bown, T.M., and Kraus, M.J., 1987, Integration of channel and floodplain suites, I. Developmental sequence and lateral relations of alluvial paleosols: Journal of Sedimentary Petrology, v. 57, p. 587-601.

Bowen, G.J., and Bloch, J.I., 1997, Petrography and Geochemistry of Floodplain Limestones From the Clarks Fork Basin , Wyoming , USA: Carbonate Deposition and Fossil Accumulation on a Paleocene – Eocene Floodplain: Journal of Sedimentary Research, v. 72, p. 46-58.

Bowen, G.J., Daniels, a. L., and Bowen, B.B., 2008, Paleoenvironmental Isotope Geochemistry and Paragenesis of Lacustrine and Palustrine Carbonates, Flagstaff Formation, Central Utah, USA: Journal of Sedimentary Research, v. 78, p. 162–174.

Breecker, D.O., Sharp, Z.D., and McFadden, L.D., 2009, Seasonal bias in the formation and stable isotopic composition of pedogenic carbonate in modern soils from central New Mexico, USA: Bulletin of the Geological Society of

America, v. 121, p. 630–640.

Cerling, T.E., 1984, The stable isotopic composition of modern soil carbonate and its relation to climate: Earth Planetary Science Letters, v. 71, p. 229–240.

Cerling, T.E., and Harris, J.M., 1999, Carbon isotopic fractionation between diet and and bioapatite in ungulate mammals and implications for ecological and paleoecological studies: Oecologica, v. 120, p. 347-363.

Cerling, T.E., and Quade, J., 1993, Stable Carbon and Oxygen Isotopes in Soil Carbonates, *in* Swart, P.K., Lohmann, K.C., McKenzie, J.A., and Savin, S. eds., Climate Change in Continental Isotopic Records, Washington, American Geophysical Union, v. Geophysica, p. 217–231.

Cerling, T.E., Solomon, D.K., Quade, J., and Bowman, J.R., 1991, On the isotopic composition of carbon in soil carbon dioxide: Geochimica et Comochimica Acta, v. 55, p. 3403-3405.

Chase, C.G., Gregory-Wodzicki, K.M., Parrish, J.T., and DeCelles, P.G., 1998, Topographic history of the Western Cordillera of North America and controls on climate: Tectonic boundary conditions for climate reconstructions, *in* Oxford Monographs on Geology and Geophysics, v. 39, p. 73–99.

Dansgaard, W., 1964, Stable isotopes in precipitation: Tellus, v. 16, p. 436–468.

Deussen, A., and Owen, D.O., 1939, Correlation of surface and subsurface formations in two typical sections of the gulf coast of Texas: Bulletin of the

American Association of Petroleum Geologists, v. 23, p. 1603-1634.

Dupont-Nivet, G., Krijgsman, W., Langereis, C.G., Abels, H.A., Dai, S., and Fang, X., 2007, Tibetan plateau aridification linked to global cooling at the Eocene–Oligocene transition: Nature, v. 445, p. 635–638.

Dworkin, S.I., Nordt, L., and Atchley, S., 2005, Determining terrestrial paleotemperatures using the oxygen isotopic composition of pedogenic carbonate: Earth and Planetary Science Letters, v. 237, p. 56–68.

Eargle, D.H., Hinds, G.W., and Weeks, A.M.D., 1971, Uranium geology and mines, South Texas, Field Trip Guidebook 12: Houston, TX, American Association of Petroleum Geologists, 59 p.

Emiliani, C., 1966, Paleotemperature analysis of Caribbean cores P6304-8 and P6304-9 and a generalized temperature curve for the past 425,000 years: Journal of Geology, v.74, p. 109-126.

Eronen, J.T., Janis, C.M., Chamberlain, C.P., and Mulch, A., 2015, Mountain uplift explains differences in Palaeogene patterns of mammalian evolution and extinction between North America and Europe.: Proceedings. Biological sciences: The Royal Society, v. 282, p. 1-8.

Ewing, T.E., and Reed, R.S., 1984, Depositional systems and structural controls of Hackberry sandstone reservoirs in Southeast Texas: University of Texas at Austin, Bureau of Economic Geology, Geological Circular 84-7, 44 p.

Fan, M., Heller, P., Allen, S.D., and Hough, B.G., 2014a, Middle Cenozoic uplift

and concomitant drying in the central Rocky Mountains and adjacent Great Plains: Geology, v. 42, p. 547–550.

Fan, M., Hough, B.G., and Passey, B.H., 2014b, Middle to late Cenozoic cooling and high topography in the central Rocky Mountains: Constraints from clumped isotope geochemistry: Earth and Planetary Science Letters, v. 408, p. 35-47.

Farquhar, G.D., Ehleringer, J.R., and Hubick, K.T., 1989, Carbon isotope discrimination and photosynthesis: Annual Reviews of Plant Physiology and Molecular Biology, v. 40, p. 503-537.

Fessenden, J.E., and Ehleringer, J.R., Temporal variations in the $\delta^{13}C$ of ecosystem respiration in the Pacific Northwest: Links to moisture stress: Oecologia, v. 136, p. 129-136.

Fox, D.L., Honey, J.G., Martin, R.A., and Pelaez-Campomanes, P., 2012a, Pedogenic carbonate stable isotope record of environmental change during the Neogene in the southern Great Plains, southwest Kansas, USA: Oxygen isotopes and paleoclimate during the evolution of C4-dominated grasslands: Bulletin of the Geological Society of America, v. 124, p. 431–443.

Fox, D.L., Honey, J.G., Martin, R.A., and Pelaez-Campomanes, P., 2012b, Pedogenic carbonate stable isotope record of environmental change during the Neogene in the southern Great Plains, southwest Kansas, USA: Carbon isotopes and the evolution of C_4-dominated grasslands: Bulletin of the

Geological Society of America, v. 124, p. 444-462.

Fox, D.L., and Koch, P.L., 2003, Tertiary history of C_4 biomass in the Great Plains, USA: Geology, v. 31, p. 809-812.

Gallagher, T.M., and Sheldon, N.D., 2016, Combining soil water balance and clumped isotopes to understand the nature and timing of pedogenic carbonate formation: Chemical Geology, v. 435, p. 79-91.

Galloway, W.E., Murphy, T.D., Belcher, R.C., Johnson, B.D., and Sutton, S., 1977, Catahoula Formation of the Texas coastal plain: Depositional systems, composition, structural development, ground-water flow history, and uranium distribution, Bureau of Economic Geology, University of Texas Report of Investigations No. 87, 59 p.

Galloway, W.E., 1982, Depositional Architecture of Cenozoic gulf coastal plain fluvial systems. Bureau of Economic Geology, University of Texas Geological Circular 82-5, 28 p.

Galloway, W.E., Jirik, L.A., Morton, R.A., and DuBar, J.R., 1986, Lower Miocene (Fleming) Depositional Episode of the Texas Coastal Plain and Continental Shelf: Structural framework, facies, and hydrocarbon resources: Bureau of Economic Geology, University of Texas Report of Investigations No. 150, 50 p.

Galloway, W.E., Ganey-Curry, P.E., Li, X., and Buffler, R.T., 2000, Cenozoic depositional history of the Gulf of Mexico basin: AAPG Bulletin, v. 84, p.

1743–1774.

Giles, L.H., Peterson, F.F., and Grossman, R.B., 1966, Morphological and genetic sequences of carbonate accumulation in desert soils: Soil Science, v. 101, p. 347-360.

Hall, J.S., Mozley, P., Davis, J.M., Roy, N.D., and Anonymous, 2004, Environments of formation and controls on spatial distribution of calcite cementation in Plio-Pleistocene fluvial deposits, New Mexico, U.S.A: Journal of Sedimentary Research, v. 74, p. 643–653.

Heintz, M.L., Yancey, T.E., Miller, B. V., and Heizler, M.T., 2014, Tephrochronology and geochemistry of eocene and oligocene volcanic ashes of east and central Texas: Bulletin of the Geological Society of America, v. 127, p. 770–780.

Hillel, D., 1980, Fundamentals of soil physics: San Diego, Academic Press, Inc., 413 p.

Hooker, J.J., Collinson, M.E., and Sille, N.P., 2004, Eocene-Oligocene mammalian faunal turnover in the Hampshire Basin, UK: calibration to the global time scale and the major cooling event: Journal of the Geological Society, v. 161, p. 161–172.

Hough, B.G., Fan, M., and Passey, B.H., 2014, Calibration of the clumped isotope geothermometer in soil carbonate in Wyoming and Nebraska, USA: Implications for paleoelevation and paleoclimate reconstruction: Earth and

Planetary Science Letters, v. 391, p. 110–120.

Huang, Y., Street-Perrott, F.A., Metcalfe, S.E., Brenner, M., Moreland, M., and Freeman, K.H., 2001, Climate change as the dominant control on glacial-interglacial variations in C_3 and C_4 plant abundance: Science, v. 293, p. 1647-1651.

Huntington, K.W., Wernicke, B.P., and Eiler, J.M., 2010, Influence of climate change and uplift on Colorado Plateau paleotemperatures from carbonate clumped isotope thermometry: Tectonics, v. 29, p. 1–19.

IAEA (2017). Global Network of Isotopes in Rivers. The GNIR Database. Accessible at: http://www.iaea.org/water

James, N.P., 1972, Holocene and Pleistocene crust (caliche) profiles. Criteria for subaerial exposure: Journal of Sedimentary Petrology, v. 42, p. 817-836.

Jury, W.A., Gardner, W.R., and Gardner, W.H., 1991, Soil Physics: New York, John Wiley and Sons, 328 p.

Kendall, C., and Coplen, T.B., 2001, Distribution of oxygen-18 and deuterium in river waters across the United States: Hydrological Processes, v. 15, p. 1363–1393.

Kim, S, and O'Neil, J, 1997, Equilibrium and nonequilibrium oxygen isotope effects in synthetic carbonates: Geochimica et Cosmochimica Acta, v. 61, p. 3461–3475.

Klappa, C.F., 1980, Rhizoliths in terrestrial carbonates: classification, recognition,

genesis and significance: Sedimentology, v. 27, p. 613-629.

Koch, P.L., Diffenbaugh, N.S., and Hoppe, K.A., 2004, The effects of late Quaternary climate and pCO_2 change on C_4 plant abundance in the south-central United States: Palaeogeography, Palaeoclimatology, Palaeoecology, v. 207, p. 331-357.

Longman, M.W., 1980, Carbonate digenetic textures from nearsurface diagenetic environments: AAPG Bulletin, v. 64, p. 461-487.

Machel, H.G., and Burton, E.A., 1991, Factors governing cathodoluminescence in calcite and dolomite and their implications for studies of carbonate diagenesis, *in* Barker, C.E., and Kopp, O.C., eds., Luminescence Microscopy and Spectroscopy: SEPM, Short Course 25, p. 37-57.

Machette, M.N., 1985, Calcic soils of the southwestern United States, *in* Weide, D.L., ed., Soils and Quaternary Geology of the Southwestern United States: Geological Society of America, Special Paper 203, p. 1-21.

Mack, G.H., Cole, D.R., and Treviño, L., 2000, The distribution and discrimination of shallow, authigenic carbonate in the pliocene-pleistocene palomas basin, Southern Rio Grande rift: Bulletin of the Geological Society of America, v. 112, p. 643–656.

McBride, E.F., Lindemann, W.L., and Freeman, P.S., 1968, Lithology and petrology of the Gueydan (Catahoula) formation in South Texas: Bureau of Economic Geology, University of Texas Report of Investigations No. 63,

122 p.

McBride, E., Picard, P.E., and Folk, R.L., 1994, Oriented concretions, Ionian Coast, Italy: Evidence of groundwater flow direction: Journal of Sedimentary Research, v.64, p. 535-540.

Mix, H.T., and Chamberlain, C.P., 2014, Stable isotope records of hydrologic change and paleotemperature from smectite in Cenozoic western North America: Geochimica et Cosmochimica Acta, v. 141, p. 532–546.

Mozley, P.S., and Davis, J.M., 2005, Internal structure and mode of growth of elongate calcite concretions: Evidence for small-scale, microbially induced, chemical heterogeneity in groundwater: GSA Bulletin, v. 117, p. 1400-1412.

Mozley, P.S., and Davis, J.M., 1996, Relationship between oriented calcite concretions and permeability correlation structure in an alluvial aquifer, Sierra Ladrones Formation, New Mexico: Journal of Sedimentary Research, v. 66, p. 11-16.

Palmquist, W.N., and Johnson, A.I., 1962, Vadose flow in layered and nonlayered materials: U.S. Geological Survey, Professional Paper P450A, p. 142-143.

Pape, J.R., Banner, J.L., Mack, L.E., Musgrove, M., and Guilfoyle, A., 2010, Controls on oxygen isotope variability in precipitation and cave drip waters, central Texas, USA: Journal of Hydrology, v. 385, p. 203–215.

Phillips, S.E., and Self, P.G., 1987, Morphology, crystallography and origin of needle-fiber calcite in Quaternary pedogenic calcretes of South Australia:

Australian Journal of Soil Research, v. 25, p. 429-444.

Quade, J., and Cerling, T.E., 1995, Expansion of C_4 grasses in the late Miocene of northern Pakistan: evidence from stable isotopes in Paleosols: Palaeogeography, Palaeoclimatology, Palaeoecology, v. 115, p. 91-116.

Quade, J., and Roe, L.J., 1999, The stable-isotope composition of early ground-water cements from sandstone in paleoecological reconstruction: Journal of Sedimentary Research, v. 69, p. 667–674.

Quast, A., Hoefs, J., and Paul, J., 2006, Pedogenic carbonates as a proxy for palaeo-CO2 in the Palaeozoic atmosphere: Palaeogeography, Palaeoclimatology, Palaeoecology, v. 242, p. 110–125.

Rabenhorst, J.A., and Wilding, P.E., 1986, Pedogenesis on the Edwards Plateau Texas, III. New model for the formation of petrocalcic horizons: Soil Science Society American Journal, v. 50, p. 693-699.

Ramstein, G., Fluteau, F., Besse, J., and Joussaume, S., 1997, Effect of orogeny, plate motion and land–sea distribution on Eurasian climate change over the past 30 million years: Nature, v. 386, p. 788–795.

Raynor, N.A., Parker, D.E., Horton, E.B., Folland, C.K., Alexander, L.V. Rowell, D.P., Kent, E.C., and Kaplan, A., 2003, Globally complete analyses of sea surface temperature, sea ice and night marine air temperature, 1871-2000: Journal of Geophysical Research, v. 108, p. 4407.

Retallack, G.J., 2001, Soils of the Past: An introduction to paleopedology, 2nd ed.:

Oxford, Blackwell Science, 404 p.

Retallack, G.J., The, S., May, N., and Retallack, G.J., 2007, Cenozoic Paleoclimate on Land in North America: Journal of Geology, v. 115, p. 271–294.

Romanek, C.S., Grossman, E.L., and Morse, J.W., 1992, Catrbon isotopic fractionation in synthetic aragonite and calcite-Effedt of temperature and precipitation rate: Geochimica et Cosmichimica Acta, v. 56, p. 419-430.

Sanyal, P., Bhattacharya, S.K., Kumar, R., Ghosh, S.K., and Sangode, S.J., 2005, Palaeovegetational reconstruction in Late Miocene: A case study based on early diagenetic carbonate cement from the Indian Siwalik: Palaeogeography, Palaeoclimatology, Palaeoecology, v. 228, p. 245–259.

Sellards, E.H., Adkins, W.S., and Plummer, F.B., 1932, The Geology of Texas: Volume 1 Stratigraphy: Univerity of Texas Bulletin No. 3232, 1018 p.

Shackleton, N.J., and Opdyke, N.D., 1976, Oxygen-isotope and paleomagnetic stratigraphy of Pacific core V28-239, late Pliocene to latest Pleistocene; Geological Society of America Memoir 145, p. 494-464.

Sheldon, N, D., and Retallack, G.J., 2004, Regional Paleoprecipitation Records from the Late Eocene and Oligocene of North America: The Journal of Geology, v. 112, p. 487–494.

Sheldon, N.D., Grimes, S.T., Hooker, J.J., Collinson, M.E., Bugler, M.J., Hren, M.T., Price, G.D., and Sutton, P.A., 2016, Coupling of marine and

continental oxygen isotope records during the Eocene-Oligocene transition: Bulletin of the Geological Society of America, v. 128, p. 502–510.

Singh, S., Parkash, B., Awasthi, A.K., and Singh, T., 2012, Palaeoprecipitation record using O-isotope studies of the Himalayan Foreland Basin sediments, NW India: Palaeogeography, Palaeoclimatology, Palaeoecology, v. 331–332, p. 39–49.

Solis, R.F.I., 1981, Upper Tertiary and Quaternary depositional systems central coastal plain, Texas: Regional geology of the coastal aquifer and potential liquid-waste repositories: Bureau of Economic Geology, University of Texas Report of Investigations No. 108, 89 p.

Sun, J., Ni, X., Bi, S., Wu, W., Ye, J., Meng, J., and Windley, B.F., 2014, Synchronous turnover of flora, fauna, and climate at the Eocene–Oligocene Boundary in Asia: Scientific Reports, v. 4, p. 7463, doi: 10.1038/srep07463.

Wade., B.S., Houben, A.J.P., Quaijtaal, W., Schouten, S., Rosenthal, Y., Miller, K.G., Katz, M.E., Wright, J.D., and Brinkuis, H., 2012, Multiproxy record of abrupt sea-surface cooling across the Eocene-Oligocene transition in the Gulf of Mexico: Geology, v. 40, p. 159-162.

Wright, V.P., Platt, N.H., Marriott, S.B., and Beck, V.H., 1995, A classification of rhizogenic (root-formed) calcretes, with examples from the Upper Jurassic-Lower Cretaceous of Spain and Upper Cretaceous of southern France: Sedimentary Geology, v. 100, p. 143-158.

Yu J, Norwine J, Bingham R, and Tebaldi C. 2006. Potential climatic deterioration in semiarid subtropical South Texas. Geography Online; 6(2). Available from: http://www.siue.edu/GEOGRAPHY/ONLINE/gov6n2.html.

Zachos, J., Pagani, M., Sloan, L., Thomas, E., and Billups, K., 2001, Trends, rhythms, and aberrations in global climate 65 Ma to present: Science, v. 292, p. 686–693.

Zhou, J., and Chafetz, H.S., 2010, Pedogenic Carbonates in Texas: Stable-Isotope Distributions and Their Implications for Reconstructing Region-Wide Paleoenvironments: Journal of Sedimentary Research, v. 80, p. 137–150.

Biographical Information

Conan Godfrey attended the University of North Carolina at Charlotte and earned a B.S. in Geology. Since attending the University of Texas at Arlington, he has worked on play-based assessments utilizing well logs, three dimensional seismic, and production data, and enjoys attending meetings of the Fort Worth Geological Society when time allows. He plans to work in the energy industry upon graduation.